https://doi.org/10.5194/essd-2026-626
Preprint. Discussion started: 8 September 2026

Open Access Earth System Science Data Discussions

A long-term wintertime snow depth dataset on Arctic sea ice (1978-2025) derived from multisource passive microwave radiometer data

Lian He[1, 2], Xinning Peng[1, 2], Yi Zhou[3], Fengming Hui[1, 2], Zhuoqi Chen[1, 2], Liangbing Chen[1, 2], Xianwei Wang[3], Xiao Cheng[1, 2]

[1]School of Geospatial Engineering and Science, Sun Yat-sen University and Southern Marine Science and Engineering Guangdong Laboratory (Zhuhai), Zhuhai, 519082, China
[2]Key Laboratory of Comprehensive Observation of Polar Environment, Sun Yat-sen University, Ministry of Education, Zhuhai, 519082, China
[3]School of Oceanography, Shanghai Jiao Tong University and Key Laboratory of Polar Ecosystem and Climate Change, Ministry of Education, Shanghai, 200030, China

Correspondence to: Xiao Cheng (chengxiao9@mail.sysu.edu.cn)

Abstract. Snow on sea ice is a key component of the Arctic climate system, strongly regulating the surface energy and mass balances of ice-covered regions. This study presents a long-term wintertime snow depth (SD) dataset on Arctic sea ice spanning the period 1978–2025 derived from multi-channel brightness temperature (TB) observations acquired by the Scanning Multichannel Microwave Radiometer (SMMR), Special Sensor Microwave/Imager (SSM/I), and Special Sensor Microwave Imager/Sounder (SSMIS). We first analysed the relationship between the spectral gradient ratio (GR) of vertically polarized TBs at 19 and 37 GHz (GRV(37/19)) and altimetric snow depth derived from the Ice, Cloud and land Elevation Satellite-2 (ICESat-2) and CryoSat-2 missions. Based on this analysis, we proposed a new SD estimation algorithm using three predictors, including GRV(37/19), bulk snow density from the NASA Eulerian Snow On Sea Ice Model (NESOSIM) and a cumulative time variable to account for the effects of snow metamorphism on passive microwave retrievals. The resulting SYSU SnowDepth dataset was validated against various independent observations, categorized into point-scale and transect-based measurements. While the dataset demonstrates an overall good accuracy, the validation performance was strongly influenced by the spatial representativeness of the reference data. Specifically, root-mean-square error (RMSE) values ranged from ~3 to 7 cm against transect-based measurements from airborne and buoy array observations, but increased to 10 to 17 cm against point-scale measurements from individual buoys, aircraft landing sites and ship-based observations. Furthermore, retrieval accuracy was higher over first-year ice (FYI) than multi-year ice (MYI) and exhibited a seasonal variation with RMSE increasing from October to April as the snowpack thickens. To our knowledge, the SYSU SnowDepth dataset is the longest satellite-based SD record providing pan-Arctic coverage of both FYI and MYI throughout the full winter season (October–April). It is expected to significantly benefit altimetry-based sea ice thickness estimation, the assimilation of snow information into sea ice models, the assessment of light availability for under-ice biota, weather forecasting, and climate monitoring. The newly developed SYSU SnowDepth dataset is available at https://doi.org/10.5281/zenodo.21472646 (He et al., 2026).

1 Introduction

Snow on sea ice is an integrated component of the polar sea ice and climate systems. Snow depth (SD) on sea ice is a critical variable that controls the mass balance of sea ice and governs the heat and energy exchange between the ocean and the atmosphere due to the high surface albedo and low thermal conductivity of snow (Perovich et al., 2002; Sturm et al., 2002). Reliable SD estimates are essential for understanding these heat flux dynamics and improving weather forecast and climate monitoring applications (Fritzner et al., 2019; Arduini et al., 2022). SD is also the major source of uncertainty in converting satellite altimeter-derived sea ice freeboards into sea ice thickness and volume estimates (Zygmuntowska et al., 2014; Sievers et al., 2024). A widely used SD dataset on Arctic sea ice is the Warren climatology (W99) (Warren et al., 1999),

https://doi.org/10.5194/essd-2026-626
Preprint. Discussion started: 8 September 2026

which was developed mainly from observations over multi-year ice (MYI) at Soviet drifting stations during 1954–1991. However, its applicability to the modern Arctic Ocean is constrained by the widespread replacement of MYI by first-year ice (FYI), and applying this outdated static snow climatology can introduce sea ice thickness biases of up to 0.5 m (Kern et al., 2015; Shi et al., 2020). In particular, replacing W99 with dynamically modelled SD fields has yielded 60–100% higher regional thinning rates and 76% greater interannual variability in observed sea-ice thickness (Mallett et al., 2021). These limitations underscore the need for a temporally consistent and spatially comprehensive long-term SD record to characterize snow variability and improve assessments of Arctic sea ice change in a warming climate (Intergovernmental Panel on Climate, 2023).

Satellite remote sensing provides the most practical means of estimating SD at hemispheric to global scale, and two main approaches can be identified: passive microwave (PMW) radiometry and dual-frequency altimetry. PMW brightness temperature (TB) observations have been employed to estimate SD for over four decades at a high temporal resolution of daily or sub-daily. The most commonly used approach for estimating SD from PMW data is the spectral gradient ratio (GR) method pioneered by (Markus and Cavalieri, 1998). The GR method relies on the frequency-dependent properties of volume scattering within the snow layer, where the TB at higher frequencies (e.g., 37 GHz) is more strongly attenuated by snowpack than at lower frequencies (e.g., 19 GHz) and the scattering increases proportionally with increasing SD. Therefore, SD can be empirically retrieved from an assumed linear relationship between GR and SD. The GR method has been applied to various PMW sensors to generate SD products using sensor-specific or updated regression coefficients. However, the GR method is generally restricted to dry snow conditions with SD below 50 cm, and its performance is also affected by snow and ice properties, such as ice type, snow density, grain size, and surface roughness, which introduce substantial spatial and temporal variability into the GR-SD relationship (Rostosky et al., 2018; Kwon et al., 2023; He et al., 2024). The evolution of SD retrieval algorithm from PMW data has primarily advanced through three key directions: the introduction of lower frequencies (such as 6.9 and 1.4 GHz) for deeper snow depths by providing better penetration (Maaß et al., 2013; Rostosky et al., 2018; Shen et al., 2022; He et al., 2022), the utilization of machine learning algorithms to model the non-linear and complex relationships between PMW-based features (e.g., TBs, GRs) and SD (Kilic et al., 2019; Braakmann-Folgmann and Donlon, 2019; Liu et al., 2019; Li et al., 2022; He et al., 2023; Zhou et al., 2026), and the consideration of features that influences the relationship between GR and SD (Kwon et al., 2023; He et al., 2024; Zhou et al., 2025; Nelson et al., 2026). Nevertheless, most SD retrieval algorithms rely on reference datasets with limited spatial and temporal coverage. This constraint hinders their transferability and accuracy outside the calibration domain.

An alternative and increasingly attracting approach involves the use of dual-frequency altimetry, which exploits the frequency-dependent penetration depth of radar waves into the snow layer. By utilizing two different frequencies, such as the combination of Ka-band (e.g., AltiKa) and Ku-band (e.g., CryoSat-2), or laser-band (e.g., ICESat-2) and Ku-band (e.g., CryoSat-2), SD can be directly and physically estimated by differentiating the freeboards measured by different frequencies with the assumption that lower frequency (i.e., Ku-band) typically reflects off the snow-ice interface in cold and dry conditions while higher frequency (laser-band or Ka-band) primarily scatters at the air-snow interface. The dual-frequency altimetry method does not inherently require any reference observations for algorithm calibration in contrast to PMW-based algorithms, and is the key technique central to the upcoming Copernicus Polar Ice and Snow Topography Altimeter (CRISTAL) mission (Landy et al., 2026). The altimetric snow depth (ASD) offers superior spatial coverages compared to traditional in situ and airborne SD measurements and provides a comprehensive reference dataset for the development of PMW-based retrieval algorithms (He et al., 2024; Zhou et al., 2025).

A variety of passive PMW radiometers have been used to generate satellite SD products. These sensors include the Scanning Multichannel Microwave Radiometer (SMMR), the Special Sensor Microwave/Imager (SSM/I), the Special Sensor Microwave Imager/Sounder (SSMIS), the Advanced Microwave Scanning Radiometer for the Earth Observing System (AMSR-E), the Advanced Microwave Scanning Radiometer 2 (AMSR2) and the Fengyun-3 (FY-3) Microwave Radiation

https://doi.org/10.5194/essd-2026-626
Preprint. Discussion started: 8 September 2026

Imager (MWRI), and have provided a long-term, basin-scale SD records at daily resolution, primarily based on the GR method. However, most PMW-based SD products derived from the 19 and 37 GHz channels are restricted to FYI. Although several SD products derived from AMSR-E and AMSR2 low frequency TB observations are available (Rostosky et al., 2018; Lee et al., 2021; He et al., 2024; Zhou et al., 2025), long-term PMW-based records extending back to the 1980s and providing pan-Arctic coverage of both MYI and FYI remain unavailable due to the lack of low frequencies (i.e., 6.9 and 10.65 GHz).

This study aims to develop an improved SD estimation algorithm based on relatively high frequencies of 19 and 37 GHz and generate a long-term wintertime (October to April) SD dataset covering both MYI and FYI across the entire Arctic Ocean using TB observations from SMMR, SSM/I, and SSMIS. To accommodate different frequency configurations between SMMR, SSM/I and SSMIS, the common frequencies of vertically polarized TBs at 19 and 37 GHz were utilized. A new SD estimation algorithm was developed based on the GR of the 19 and 37 GHz vertically polarized TBs, i.e., GRV(37/19), and subsequently validated against to various SD observations. The remainder of this paper is organized as follows. Section 2 describes the datasets, while Section 3 presents the newly developed SD estimation method. Section 4 provides the SD estimation results, followed by accuracy evaluation results in Section 5. Discussions on retrieval accuracy and potential uncertainties are presented in Section 6. Code and data availability, and conclusions are presented in Section 7 and Section 8, respectively.

2 Data

2.1 Brightness temperature observations

Brightness temperature measurements from a series of PMW radiometers including SMMR, SSM/I, and SSMIS were used for estimating SD on Arctic sea ice. SMMR onboard Nimbus-7 satellite was a ten-channel microwave sensor that measured both horizontally and vertically TBs at five frequencies (6.6, 10.7, 18.0, 21.0, and 37.0 GHz) at an incidence angle of 50.3°. The SMMR TB dataset covers the period of October 25, 1978 to August 20, 1987. The SSM/I sensor aboard the Defense Meteorological Satellite Program (DMSP) F8, F10, F11, and F13 platforms was a seven-channel PMW radiometer that measured TBs at frequencies of 19.35, 22.235, 37.0, and 85.5 GHz with an incidence angle of around 53°. The 22.235 GHz channel is measured only in vertical polarization, while the others measure in both vertical and horizontal polarizations. Only TB observations from F8 (September 7, 1987 to December 30, 1991), F11 (December 3, 1991 to September 30, 1995), and F13 (May 3, 1995 to December 31, 2008) were utilized. The SSMIS sensor onboard DMSP F15, F16, F17, and F18 platforms is a conically scanning PMW radiometer with a 53.1° Earth incidence angle at 24 channels covering a wide range of frequencies from 19 GHz to 183 GHz. TB observations from F17 (November 4, 2006 to present) were utilized. The TB datasets achieved by NSIDC were employed with the dataset IDs being NSIDC-0001 (Gloersen, 2006) and NSIDC-0007 (Meier et al., 2021), respectively. These datasets provide daily gridded TBs with a grid size of 25 km in a polar stereographic projection, and only vertically polarized TBs at 19 GHz and 37 GHz (i.e., TB19V and TB37V) were used for SD estimation in this study. The noise-equivalent temperatures (NeΔT), which stand for the uncertainty of an individual measurement, vary by sensor. For SMMR, the NeΔT values are 1.2 K and 1.5 K for TB19V and TB37V, respectively. These values decrease to 0.45 K and 0.37 K for SSM/I, and further improve to 0.34 K and 0.24 K for SSMIS.

https://doi.org/10.5194/essd-2026-626
Preprint. Discussion started: 8 September 2026

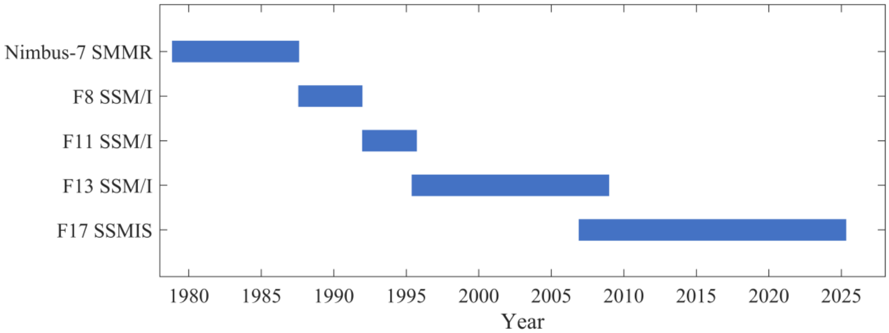

Figure 1. Time series of brightness temperature observations used in this study

Inter-calibration of SMMR, SSM/I, and SSMIS TB observations is critical to ensure a continuous, homogenized Arctic SD product dating back to 1978 since these sensors have varying viewing geometries, frequencies, bandwidths, and calibration schemes. The conventional linear regression model was used to perform the inter-calibration based on the daily gridded TBs (Dai et al., 2015), and overlap periods are used to calculate inter-sensor regression coefficients (slope and intercept). For Nimbus-7 SMMR and F8 SSM/I, the overlap period is between July 9, 1987 and August 20, 1987. For F8 SSM/I and F11 SSM/I, the overlap period is from December 3, 1991 to December 30, 1991. For F11 SSM/I and F13 SSM/I, the overlap period is from May 3, 1995 to December 30, 1995. For F13 SSM/I and F17 SSMIS, the overlap period is between October 1, 2007 and April 29, 2009 (only wintertime i.e., October to April, was applied). Since this study only focuses on the sea ice covered areas, only pixels with sea ice concentration (SIC) greater than 85% were used to calculate the regression coefficients. Table 1 summarizes the calibration coefficients. The target sensor represents the sensor that will be inter-calibrated to the reference sensor.

Table 1. Calibration coefficients between different sensor combinations

Reference sensor	Target sensor	Channel	Slope	Intercept	RMSE (K)	R^2
F8 SSM/I	Nimbus-7 SMMR	TB19V	0.8755	39.6391	2.45	0.81
		TB37V	1.1108	-23.2449	4.80	0.82
F11 SSM/I	F8 SSM/I	TB19V	0.9950	1.4180	1.24	0.99
		TB37V	1.0023	-0.0063	1.94	0.99
F13 SSM/I	F11 SSM/I	TB19V	1.0007	0.1640	1.39	0.98
		TB37V	0.9934	1.5123	2.77	0.97
F17 SSMIS	F13 SSM/I	TB19V	0.9731	3.8627	0.86	0.99
		TB37V	1.0023	0.3377	1.07	1.00

2.2 Altimetric snow depth dataset

In this study, altimetric snow depth (ASD) estimates on Arctic sea ice derived from combined ICESat-2 (IS-2) and CryoSat-2 (CS-2) freeboards were employed as the reference data to train the PMW-based GR model. The ASD product is based on taking the difference between IS-2 total freeboard (defined as the height of the air-snow interface above the local sea surface) and CS-2 ice freeboard (defined as the height of the snow-ice interface above the local sea surface) and accounting for the propagation delay through the snow layer (Kwok and Markus, 2018; Kwok et al., 2020; Kacimi and Kwok, 2022a). The SD retrievals were found to be within a few centimetres of Operation IceBridge (OIB) airborne SD measurements (Kwok et al., 2020). The IS-2 and CS-2 ASD product covers the period between October 2018 and April 2021 and has a temporal

https://doi.org/10.5194/essd-2026-626
Preprint. Discussion started: 8 September 2026

resolution of one month. It is provided on the NSIDC Sea Ice Polar Stereographic North at a spatial resolution of 25 km and is available at (Kacimi and Kwok, 2022b).

2.3 Auxiliary data

2.3.1 Snow density

Snow density is a critical parameter that influences the relationship between GR and SD (He et al., 2024). Since in situ snow density measurements on Arctic sea ice are scarce, snow density reanalysis data from the NASA Eulerian Snow on Sea Ice Model (NESOSIM) (Petty et al., 2018) were utilized. NESOSIM can simulate key processes of snow accumulation, wind packing, blowing snow, and redistribution of snow due to sea ice motion with the forcing data and can produce daily basin-wide estimates of snow depth and density on Arctic sea ice with a temporal coverage spanning from September 1980 to April 2025. For the period before April 1980, a snow density climatology dataset derived from NESOSIM was used instead. The NESOSIM data are provided on a 100 km north polar stereographic grid and were resampled to 25 km resolution using a linear interpolation method.

2.3.2 Sea ice concentration

Sea ice concentration (SIC) product was used to correct the contamination of open water within a 25 km pixel when the SIC is less than 100%. The NOAA/NSIDC Climate Data Record of Passive Microwave Sea Ice Concentration product (Meier et al., 2026) was used. This SIC data set is a fusion product which combines SIC estimates from NASA Team (NT) (Cavalieri et al., 1984) and Bootstrap (BT) (Comiso, 1986) algorithms, and starts from October 25, 1978 on a daily basis. This data covers both the Northern and Southern polar regions at a spatial resolution of 25 km.

2.3.3 Sea ice type

It is necessary to distinguish between FYI and MYI for accurate SD estimation due to their distinct ice and snow properties (Rostosky et al., 2018). The sea ice type (SITY) data distributed by Copernicus Climate Change Service (C3S) were utilized (Aaboe et al., 2023). This SITY product defines sea ice type as FYI, MYI, and ambiguous ice (AMI), where are derived from TBs measured by satellite passive microwave radiometers (i.e., SMMR, SSM/I and SSMIS). This dataset is delivered on a Lambert Azimuthal Equal Area polar projection with a grid size of 25 km and was reprojected to the 25 km NSIDC Sea Ice Polar Stereographic North projection using the nearest neighbour resampling method.

2.4 Existing PMW snow depth products

Three PWM-based SD products are used for inter-comparison in this study. The first product is derived from SMMR and SSM/I data (1978–2018) based on GRV(37/19) (Markus and Cavalieri, 1998) and distributed by the NASA Goddard Space Flight Centre (GSFC) (referred to as GSFC SnowDepth). The GSFC SnowDepth product is available on a daily basis with a spatial resolution of 25 km. The second product is derived from AMSR-E/2 data (2002–2025) based on GRV(37/19) (Comiso et al., 2003) and archived by NSIDC (referred to as NSIDC SnowDepth). The NSIDC SnowDepth product has a spatial resolution of 12.5 km and was averagely aggregated to 25 km to match other SD products. Both the GSFC SnowDepth and NSIDC SnowDepth products have no SD retrievals over MYI. The third product is derived from AMSR-E/2 data (2002–2025) based on the GR of the 6.9 GHz and 18.7 GHz vertically polarized TBs (i.e., GRV(19/7)) (Rostosky et al., 2018) and is available at the University of Bremen (referred to as Bremen SnowDepth). The Bremen SnowDepth product has a spatial resolution of 25 km and a temporal resolution of one day. For the Bremen SnowDepth product, SD is derived from November to April over FYI and from March to April for MYI.

https://doi.org/10.5194/essd-2026-626
Preprint. Discussion started: 8 September 2026

2.5 Snow depth measurement datasets

2.5.1 Airborne snow depth measurements

The airborne SD observations were obtained from the NASA's OIB mission and the Alfred Wegener Institutes (AWI) IceBird campaign series. The OIB SD data set contains two parts, IceBridge L4 Sea Ice Freeboard, Snow Depth, and Thickness, Version 1 (IDCSI4) (referred to as OIB-NSIDC) (Kurtz et al., 2015) and IceBridge Sea Ice Freeboard, Snow Depth, and Thickness Quick Look, Version 1 (NSIDC-0708) (referred to as OIB-GSFC) (Kurtz et al., 2016). The OIB-NSIDC data set contains derived geophysical data products including sea ice freeboard, snow depth, and sea ice thickness measurements in Arctic retrieved from IceBridge Snow Radar, Digital Mapping System (DMS), Continuous Airborne Mapping By Optical Translator (CAMBOT), and Airborne Topographic Mapper (ATM) data sets. The OIB-GSFC data set is the Quick Look counterpart to the OIB-NSIDC data set and is an evaluation product. The OIB-NSIDC and OIB-GSFC were mainly conducted in Spring (March and April) and covered regions mainly in the Beaufort Sea, the Greenland Sea and the Central Arctic Ocean.

For the AWI IceBird campaign series, airborne SD measurements on sea ice were conducted during the Polar Airborne Measurements and Arctic Regional Climate Model Simulation Project (PAMARCMIP) (Jutila et al., 2024b) in April 2017 and during the IceBird Winter 2019 campaign (Jutila et al., 2024a) in April 2019. The data consist of several surveys spanning sea-ice covered areas in the Beaufort Sea, Chukchi Sea, Lincoln Sea, and Central Arctic Ocean and are referred to as AWI IceBird. The spatial distribution of the three OIB-NSIDC, OIB-GSFC, and AWI IceBird SD measurements is displayed in Figure 2, and the spatial resolution is about 40 m between each measurement. The airborne SD measurements were averagely gridded into on the 25 km NSIDC polar stereographic grid. In order to avoid a small fraction of the 25 km grid intersected by airborne SD observations, only the grid cells with a sufficient length of SD measurements were selected (Rostosky et al., 2018). In this study, the threshold length of SD transects within a 25 km pixel was set as 10 km, and the influence of transect length on evaluation metrics was investigated in Section 6.

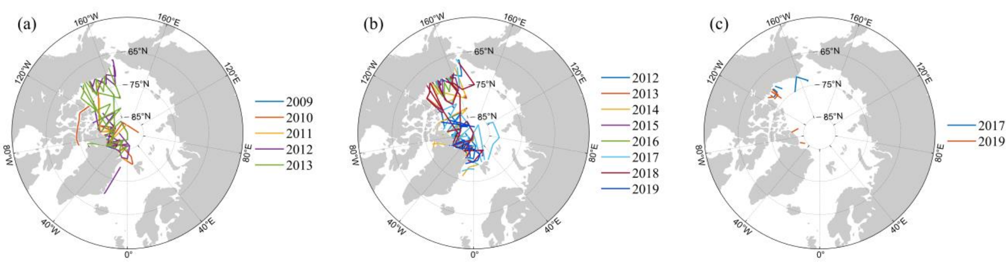

Figure 2. Spatial distribution of airborne snow depth measurements from (a) OIB-NSIDC (2009–2013), (b) OIB-GSFC (2012–2019), and (c) AWI-IceBird (2017 and 2019).

2.5.2 Buoy snow depth measurements

Three types of buoy-based SD measurements were collected, including the Ice Mass Balance (IMB) buoy (Perovich et al., 2022), the snow buoy (SB) (Nicolaus et al., 2017) and the Snow and Ice Mass Balance Apparatus (SIMBA) buoy (Preußer et al., 2025). The spatial distribution of buoy measurements is shown in Figure 3. The IMB buoy is an autonomous, ice-based system developed at the Cold Regions Research and Engineering Laboratory (CRREL) and records the thermodynamic changes in sea ice, including measurements of ice temperature, ice growth, ice thickness, and snow depth at a single point on an ice floe. A total of 45 IMB buoys (as indicated in Table A1) were collected during the period of 2002 to 2015 and covered areas in the Arctic Ocean and the Beaufort Sea. Current and historical IMB datasets are actively tracked by the CRREL-Dartmouth Mass Balance Buoy Program and are referred to as CRREL IMB. The SB buoys primarily measure the snow

https://doi.org/10.5194/essd-2026-626
Preprint. Discussion started: 8 September 2026

thickness atop sea ice by using ultrasonic echo sounders to continuously detect the distance to the snow cap. A total of 48 SB buoys (as indicated in Table A2) were collected for the period of 2013 to 2024. The SB dataset is publicly accessible via the Meereisportal and is referred to as AWI SB. The SIMBA buoys (as indicated in Table A3) measure SD and ice thickness using a vertical string of highly precise thermistors that track temperature gradients across the air-snow-ice-ocean column. With sensors spaced every 2 cm, they map the boundaries where snow, ice, and water meet to yield SD data with an accuracy of ± 2 cm. All the buoys collected SD data at an interval of several hours. The high temporal resolution SD measurements were averaged to daily values to match the daily PMW TB observations. These three buoy datasets were used to validate SD individually.

In addition, the MOSAiC expedition employed a distributed network of autonomous buoys to sea ice and snow parameters centred the MOSAiC Central Observatory (CO) within a radius of ~50 km (Rabe et al., 2024). The MOSAiC buoy array contains 21 buoys (as indicated in Table A4) from October 2019 to April 2010, including 13 SIMBA buoys (Lei et al., 2021), 5 snow buoys (Nicolaus et al., 2022) and 3 seasonal ice mass balance (SIMB) buoys (Perovich et al., 2023). It should be noted that these 13 SIMBA buoys and 5 AWI snow buoys were integrated into the MOSAiC buoy network and were excluded from the subsequent validation using individual buoys. For each day, SD measurements from the above 21 buoys were averaged spatially to align with the PMW 25 km grid. The trajectory of MOSAiC buoy network is displayed in Figure 3(d). Meanwhile, sea ice and snow measurements from year-long transects at the MOSAiC CO were also collected (Itkin et al., 2023). More details about the MOSAiC SD measurements are available at (Zhou et al., 2025).

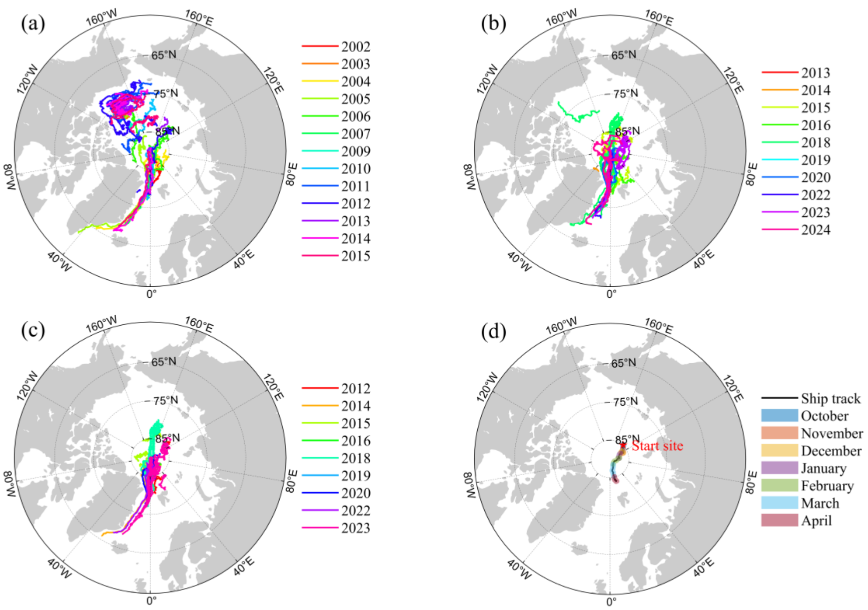

Figure 3. Spatial distribution of buoy snow depth measurements from (a) CRREL IMB (2003–2015), (b) AWI SB (2014–2018), (c) SIMBA (2012–2023), and (d) MOSAiC (only wintertime, October 2019 to April 2020).

2.5.3 Aircraft landing and ship-based snow depth measurements

Two types of in situ SD datasets were collected, including aircraft landing observations from the Former Soviet Union (Romanov, 2004) and ship-based observations from the ASSIST/IceWatch protocol (Hutchings et al., 2018; Kern, 2020). The former dataset contains sea ice and snow measurements collected during aircraft landings associated with the Soviet Union's historical Sever airborne and North Pole drifting station programs. In this study, a total of 408 data points were selected spanning 1979 to 1988. This dataset primarily covers the Chukchi sea, East Siberian Sea, Laptev Sea during March and April, and constitutes the earliest dataset available for SD validation. The second dataset (referred to as

https://doi.org/10.5194/essd-2026-626
Preprint. Discussion started: 8 September 2026

ASSIST/IceWatch) comprises hourly visual SD observations conducted manually from ship bridges during cruises through sea ice, covering an approximate radius of 1 km around the vessel. This dataset was collected between 2003 and 2018, primarily during October and from January to April, and covers the Beaufort Sea, the Bering Sea, and the waters surrounding the Svalbard Archipelago. Unlike the aircraft landing dataset, the ship-based observations frequently contain multiple data points within a single 25-km PMW grid cell due to its relatively high temporal resolution.

3 Method

3.1 Snow depth estimation algorithm

In order to generate a long-term SD product dating back to 1978, the common frequencies of 19 GHz and 37 GHz of SMMR, SSM/I and SSMIS are used and the GR of the 19 GHz and 37 GHz vertically polarized TBs was used for SD estimation, with the GRV(37/19) defined as:

$$GRV(37/19) = \frac{TB(37V) - TB(19V) - k_1(1-C)}{TB(37V) + TB(19V) - k_2(1-C)} \tag{1}$$

where TB(19V) and TB(37V) indicate the brightness temperatures at 19 GHz and 37 GHz, respectively; C represents the sea ice concentration; k_1 and k_2 are terms for correcting the effect of open water in a pixel when C is less than 1 in a grid cell and can be written as:

$$k_1 = TB_{OW}(37V) - TB_{OW}(19V) \tag{2}$$

$$k_2 = TB_{OW}(37V) + TB_{OW}(19V) \tag{3}$$

where $TB_{OW}(19V)$ and $TB_{OW}(37V)$ are the open water (OW) brightness temperatures at vertical polarization of 19 GHz and 37 GHz, respectively. $TB_{OW}(19V)$ and $TB_{OW}(37V)$ are used as constants and are set as 176.99 K and 207.48 K, respectively, according to (Ivanova et al., 2015).

After the calculation of GRV(37/19), the SD on Arctic sea ice can be estimated by considering the influence of snow density ρ_{snow} (He et al., 2024) and the thermodynamic evolution of sea ice and snow (Kwon et al., 2023; Zhou et al., 2025):

$$SD(cm) = a \times GRV(37/19) + b \times \rho_{snow} + c(D) \tag{4}$$

where SD indicates the SD in centimetres; ρ_{snow} is the snow density in the unit of g/cm^3 from NESOSIM; *a*, *b*, and *c* are the regression coefficients while *c*(*D*) is the function of time factor *D* and has the form similar to (Kwon et al., 2023; Zhou et al., 2025):

$$c(D) = c_3 \times D^3 + c_2 \times D^2 + c_1 \times D + c_0 \tag{5}$$

where *D* is the cumulative time variable and represents the days from October 1.

There are six unknown parameters (i.e., a, b, c_3, c_2, c_1, c_0) to be determined using the coincident PMW GRV(37/19) and altimetric SD estimates. Two sets of coefficients are determined separately for FYI and MYI.

3.2 Uncertainty of snow depth estimates

According to Gaussian error propagation, the uncertainty of the retrieved snow depth σ_{SD} is given by

$$\sigma_{SD} = \sqrt{\sigma_a^2 \times GR^2 + a^2 \times \sigma_{GR}^2 + \sigma_b^2 \times \rho_{snow}^2 + b^2 \times \sigma_{\rho_{snow}}^2 + \sigma_c^2(D)} \tag{6}$$

where σ_a, σ_b and σ_c indicate the uncertainties of the regression coefficients; σ_{GR} indicates the uncertainty of the GRV(37/19); $\sigma_{\rho snow}$ indicates the uncertainty of snow density; σ_c(D) represents the uncertainty of the intercept and has the form:

$$\sigma_c(D) = \sqrt{\sigma_{c_3}^2 \times D^6 + \sigma_{c_2}^2 \times D^4 + \sigma_{c_1}^2 \times D^2 + \sigma_{c_0}^2 + \sigma_D^2 \times \left(3c_3 \times D^2 + 2c_2 \times D + c_1\right)^2} \tag{7}$$

where σ_{c0}, σ_{c1}, σ_{c2}, σ_{c3}, and σ_D represent the uncertainties of regression coefficients c_0, c_1, c_2, c_3 and D.

https://doi.org/10.5194/essd-2026-626
Preprint. Discussion started: 8 September 2026

4 Snow depth estimation results

4.1 Determination of regression coefficients

A total of 21 months' (covering 3 winter seasons of 2018/19, 2019/20, and 2020/21) coincident GRV(37/19) and ASD measurements were collected. The numbers of data points are about 93000 and 65000 for FYI and MYI, respectively. The GRV(37/19) values vary from −0.0217 (1% percentile) to 0.0053 (99% percentile) with a median value of -0.0067 for FYI and range from −0.0886 (1% percentile) to −0.0183 (99% percentile) with a median value of −0.0503 for MYI. The snow depths range from 3.30 cm (1% percentile) to 24.55 cm (99% percentile) with a median value of 12.37 cm for FYI and vary between 9.40 cm (1% percentile) and 39.21 cm (99% percentile) with a median of 21.81 cm for MYI. FYI has higher GRV(37/19) values and lower snow depths than MYI. For each month (October to April), the robust Huber linear regression (Huber, 1981) was used to determine the empirical linear relationship between SD and GRV(37/19). Figure 4 displays the regression models for seven separate months together with the histogram distributions of SD and GRV(37/19). Table II summarizes the correlation *r* and root mean-square error (RMSE) values between altimetric snow depth and GRV(37/19), and the number of available data points (*N*) for regression is also presented.

For both FYI and MYI, the regression models deviate from each other for different months, inferring that regression models trained on a single month of data severely limit their ability to generalize and lead to high divergence when applied to other months. The intercept values show an obvious upward trend from October to April. The intercept increases from about 5.6 cm in October/November to 14.5 cm in April for FYI, while it increases from about 8.8 cm in October/November to 19.7 cm in April for MYI. In contrast, the slope exhibits less variation over time than the intercept with the slope values varying around -219.67 ± 70.49 for FYI and around -175.52 ± 25.83 for MYI. The temporal dependence of the relationship between GRs and SD agrees well with previous studies and can be associated with snow accumulation, snow density and grain size (Kwon et al., 2023; He et al., 2024; Zhou et al., 2025).

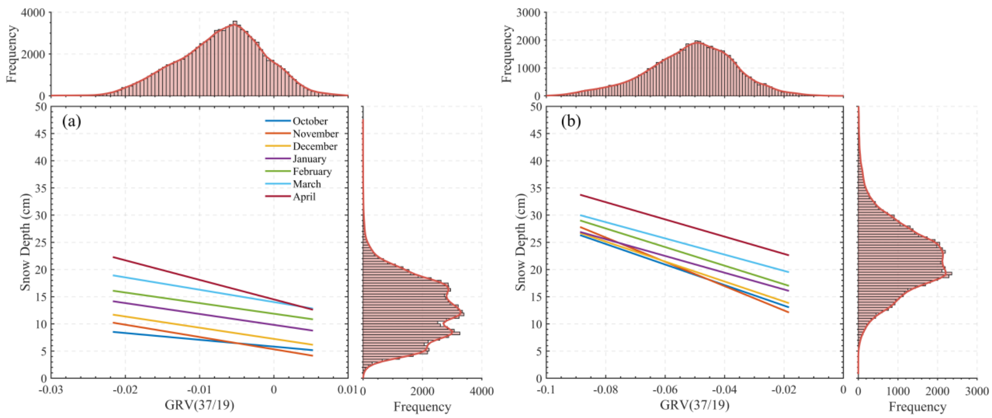

Figure 4. Regression models between snow depth and GRV(37/19) for different months over (a) FYI and (b) MYI.

According to Table 2, the mean correlation values across seven months between GRV(37/19) and ASD are about 0.38 and 0.44 for FYI and MYI, respectively, and the average RMSE values are about 2.63 cm and 4.60 cm for FYI and MYI, respectively. The relatively low RMSE values indicate that GRV(37/19) has great potential for SD estimation. Generally, FYI has lower RMSE values than MYI for each respective month, inferring that SD can be more accurately estimated on FYI than that on MYI. The RMSE values between GRV(37/19) and ASD are slightly higher than those between GRV(19/7) and ASD (2.44 cm for FYI and 3.88 cm for MYI) as indicated in (He et al., 2024), indicating that GRV(37/19) is inferior to GRV(19/7) in SD estimation, which agrees with the findings in (Rostosky et al., 2018). Although GRV(37/19) is not the best feature for SD estimation on Arctic sea ice, it is still the optimal choice considering long time series of SMMR, SSM/I and SSMIS TB data with both 19 GHz and 37 GHz channels dating back to 1978. In addition, the RMSE values for FYI display

https://doi.org/10.5194/essd-2026-626
Preprint. Discussion started: 8 September 2026

a clear upward trend from October to April as snow depths increase while the RMSE values for MYI are stable around 4.60 cm, which may infer that the GRV(37/19) is more suitable for shallow SD estimation.

Table 2. Correlation (r), RMSE (cm) and Bias (cm) between GRV(37/19) and altimetric snow depths, as well as the number (N) of available data points for each month

Month	FYI				MYI			
	r	RMSE (cm)	Bias (cm)	*N*	*r*	RMSE (cm)	Bias (cm)	*N*
October	0.25	1.90	-0.29	485	0.34	5.68	-0.71	11700
November	0.42	1.65	0.03	11001	0.47	4.82	-0.61	11127
December	0.45	1.93	-0.04	15132	0.47	4.41	-0.61	10040
January	0.41	2.52	0.01	16988	0.48	4.23	-0.54	9263
February	0.34	3.29	-0.05	16360	0.52	3.99	-0.57	8733
March	0.35	3.37	0.08	16795	0.44	4.13	-0.56	7973
April	0.43	3.72	0.06	16585	0.36	4.92	-0.71	6104
ALL	0.51	4.41	-0.14	93346	0.48	5.37	-0.48	64940

Based on the above results, an improved SD estimation algorithm was proposed as in Equation (4) and (5) by considering the temporal dependence of the linear relationship between GRV(37/19) and SD, and the influences of snow density (Kwon et al., 2023; He et al., 2024; Zhou et al., 2025). With the coincident GRV(37/19) and ASD data, the six regression coefficients (i.e., a, b, c_0, c_1, c_2, and c_3) were determined. In order to investigate the interannual variability of regression coefficients, one year's data were excluded and the remaining two years' data were used to determine the regression coefficients.

Table 3 summarizes the regression coefficients (i.e., a, b, c_0, c_1, c_2, and c_3), correlation coefficients (r), RMSE and sample sizes (N) for FYI and MYI. The results using all years' data (ALL) are also presented. The regression models achieved average correlations of 0.81 for FYI and 0.66 for MYI, with corresponding mean RMSE values of 3.00 cm and 4.62 cm. A comparison between Table 2 and Table 3 reveals that incorporating snow density and time variable D significantly improves model accuracy for all years' data (ALL). Specifically, for FYI, the RMSE decreased from 4.41 cm in Table 2 to 3.01 cm in Table 3 while r increased from 0.51 to 0.81. Similarly, MYI RMSE decreased from 5.37 cm to 4.65 cm as r increased from 0.48 to 0.65. The proposed SD retrieval algorithm in this study outperforms traditional linear models by yielding lower RMSEs and higher correlations, underscoring the critical value of integrating external snow density and time variable D.

Table 3. Regression coefficients and number of available data points over FYI and MYI

Ice Type	Excluded Year	*a*	*b*	c_0	c_1	c_2	c_3	*r*	RMSE	N
FYI	2018/19	-199.89	7.35	3.51	-2.67E-2	7.50E-4	-1.84E-6	0.81	2.89	61526
	2019/20	-195.22	3.96	3.86	-2.59E-2	9.75E-4	-2.84E-6	0.81	3.10	63424
	2020/21	-265.44	7.03	3.61	-2.36E-2	7.40E-4	-1.83E-6	0.82	2.98	61742
	ALL	-216.45	6.52	3.55	-2.54E-2	8.20E-4	-2.16E-6	0.81	3.01	93346
MYI	2018/19	-147.75	21.74	4.98	1.16E-2	-6.75E-5	1.17E-6	0.66	4.31	44348
	2019/20	-185.00	-64.01	26.43	9.32E-2	-4.19E-4	1.54E-6	0.65	4.68	39137
	2020/21	-173.37	3.05	10.21	-1.64E-2	2.27E-4	5.41E-7	0.66	4.82	46395
	ALL	-173.73	-15.80	14.33	3.26E-2	-1.17E-4	1.18E-6	0.65	4.65	64940

In conclusion, the respective regression equations for FYI and MYI are given below as:

$$SD_{FYI}\left(cm\right) = -216.45 \times GRV\left(37/19\right) + 6.52 \times \rho_{snow} - 2.16 \times 10^{-6} \times D^3 + 8.20 \times 10^{-4} \times D^2 - 2.54 \times 10^{-2} \times D + 3.55 \quad (8)$$

$$SD_{MYI}\left(cm\right) = -173.73 \times GRV\left(37/19\right) - 15.80 \times \rho_{snow} + 1.18 \times 10^{-6} \times D^3 - 1.17 \times 10^{-4} \times D^2 + 3.26 \times 10^{-2} \times D + 14.33 \quad (9)$$

The above equations are valid from October 1 to April 30 for dry snow. For AMI, SD is calculated as the average value of FYI and MYI values, as AMI generally represents a mixture of FYI and MYI.

https://doi.org/10.5194/essd-2026-626
Preprint. Discussion started: 8 September 2026

4.2 Snow depth estimates with uncertainty

By combining SMMR, SSM/I and SSMIS TB data with NOAA/NSIDC SIC, NESOSIM snow density, and C3S SITY, we generated a long-term Arctic sea ice SD dataset, hereafter referred to as the SYSU SnowDepth dataset. The uncertainty in the SD estimates was also calculated. According to (Rostosky et al., 2018), the total uncertainty consists of two components: the uncertainty stemming from small sample sizes and interannual variability, and the uncertainty inherent in the contributing input parameters. For the first component, the uncertainties were calculated from the standard deviation of the regression coefficients over the four results as indicated in Table 3. The uncertainties (σ_a, σ_b, σ_{c0}, σ_{c1}, σ_{c2}, σ_{c3}) are (32.11, 1.54, 0.15, 1.34E-3, 1.08E-4, 4.72E-7) for FYI and (15.76, 36.84, 9.14, 4.65E-2, 2.64E-4, 4.15E-7) for MYI. For the second component, the uncertainties (σ_a, σ_b, σ_{c0}, σ_{c1}, σ_{c2}, σ_{c3}) are standard outputs of the regression models using all years' data (ALL), and are (1.45, 0.47, 0.14, 3.05E-3, 2.70E-5, 7.39E-8) for FYI and (1.46, 2.20, 0.55, 4.26E-3, 4.12E-5, 1.28E-7) for MYI. The uncertainty of GRV(37/19) is calculated using the Gaussian error propagation model following (Rostosky et al., 2018). The uncertainties of the observed TBs for TB19V and TB37V are set as the NeΔT values as indicated in Section 2.1. The uncertainties of SIC, snow density and time variable D are set as 5% (Rostosky et al., 2018), 0.1 g/cm^3 and 15, respectively.

Figure 5 displays the spatial distributions of monthly averaged SD from SYSU dataset for seven months during the winter season of 2016/2017 (first row) together with their corresponding uncertainties (second row). As a comparison, SD estimates from Bremen (third row) and GSFC (fourth row) datasets are also shown. For the SYSU dataset, at the beginning of the sea ice advance in October 2016, most of the region was covered by MYI, which held a higher mean SD (15.93 cm) than FYI (6.27 cm). As the sea ice thickened and snow accumulated, SD steadily increased. By the end of the sea ice growth season in April 2017, the mean snow depths had risen to approximately 17.81 cm on FYI and 27.30 cm on MYI. The SD uncertainties also show an obvious upward trend and increase from 1.97 cm in October 2015 to 7.29 cm in April 2017. MYI typically exhibits greater uncertainty than FYI, with a difference of approximately 1.2 cm, which is consistent with the results in Table 2 and Table 3 that FYI yields more accurate SD estimates than MYI.

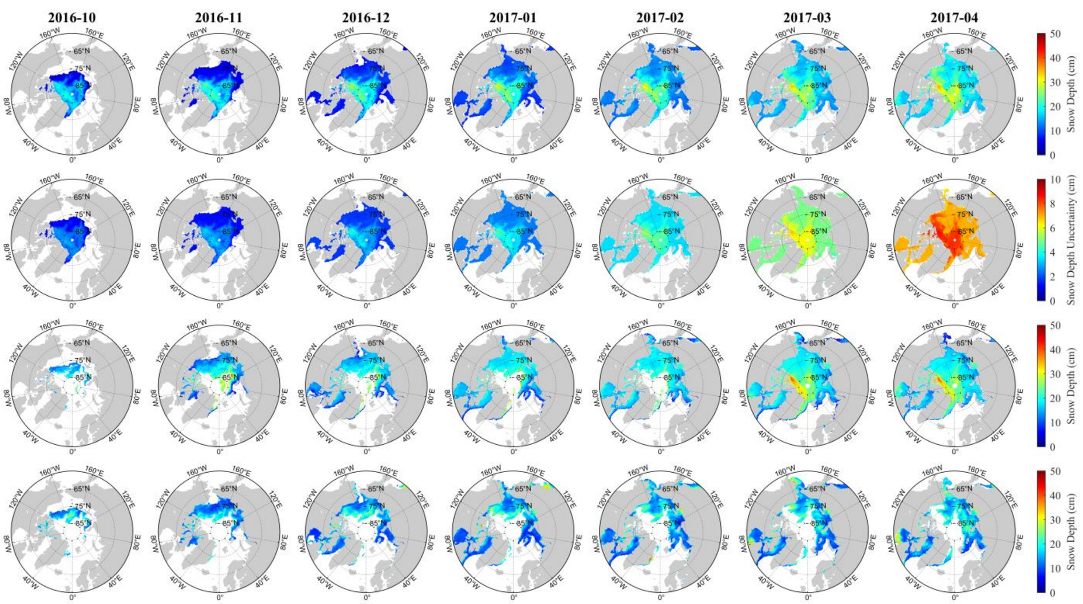

Figure 5. Spatial distribution of monthly averaged snow depths on Arctic sea ice developed in this study (first row) and their uncertainties (second row), Bremen SnowDepth (third row) and GSFC SnowDepth (fourth row) for October to April during the winter season of 2016/17.

https://doi.org/10.5194/essd-2026-626
Preprint. Discussion started: 8 September 2026

In terms of comparison between different SD datasets, both Bremen and GSFC fail to provide SD estimates on MYI for most of the winter period (October to April), with the sole exception of March and April in the Bremen dataset. In contrast, SYSU is the only dataset that offers continuous SD estimates across the entire Arctic (covering both FYI and MYI) for the full winter season. Furthermore, both Bremen and GSFC exhibit lower seasonal snow accumulation than SYSU. From October to April, mean snow depths on FYI increased from 15.86 cm to 16.96 cm for GSFC, and from 15.01 cm to 16.59 cm for Bremen. However, the mean SD on FYI for SYSU exhibited a much steeper increase, rising from 6.27 cm to 17.81 cm, which aligns more closely with expected physical patterns of snow accumulation.

4.3 Snow depth climatology on Arctic sea ice

Figure 6 shows the monthly mean SD averaged over five different decades, including 1980s (1980–1989), 1990s (1990–1999), 2000s (2000–2009), 2010s (2010–2019), and 2020s (2020–2025). Across all five decades, snow depths exhibit an increasing trend from October to April, aligning well with the seasonal variation shown in Figure 5. For example, during the 1980s, the mean SD increased from 12.93 cm in October to 22.65 cm in April. Furthermore, an overall downward trend is evident across all individual months over the past five decades. While sea ice extent shows a notable reduction in October, mean SD fluctuates around 13.29 cm with only a slight decline from the 1980s to the 2020s, as MYI dominates during this month. For the remaining months (November to April), the replacement of MYI with FYI corresponds to a more pronounced decline in mean SD with an average rate of approximately -0.60 cm/decade. For example, the mean SD for April dropped from 22.65 cm in the 1980s to 19.59 cm in the 2020s, at a rate of -0.74 cm/decade. This overall decline aligns well with earlier findings in (Webster et al., 2019; Lee et al., 2021) although the magnitude of the decrease differs. The SYSU SnowDepth dataset offers an independent benchmark for evaluating spatio-temporal variations in Arctic sea ice snow depth.

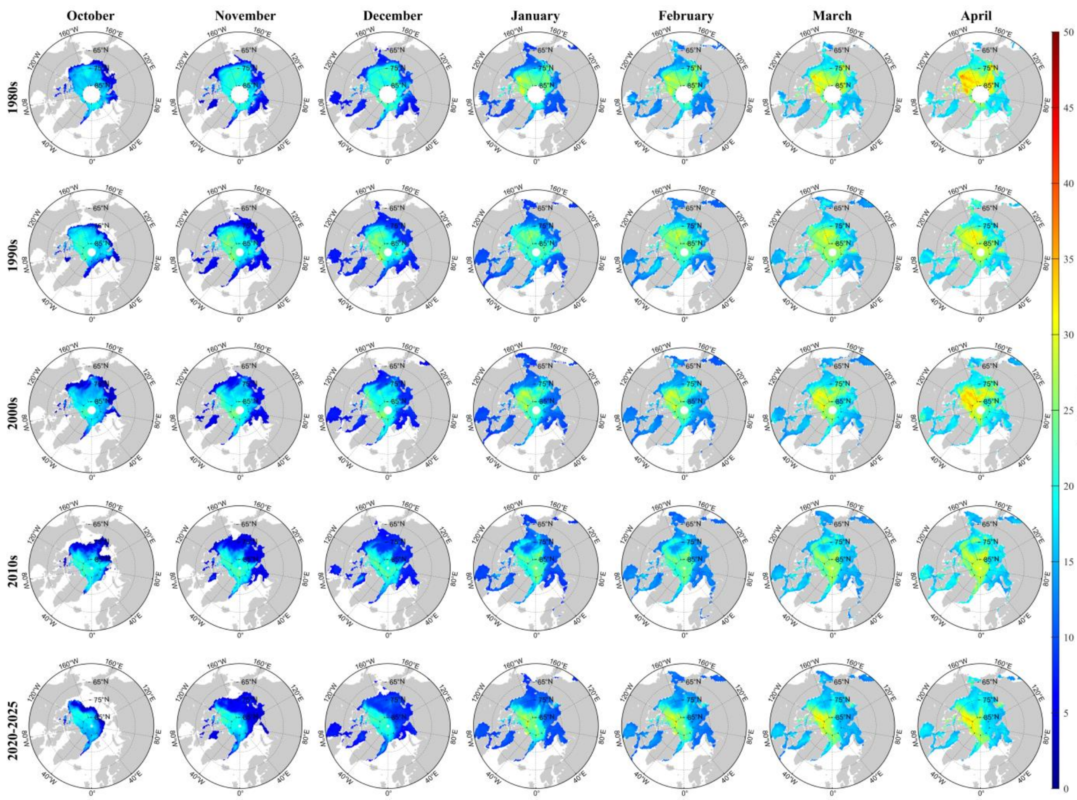

Figure 6. Spatial distribution of monthly averaged snow depths over the time period of five decades from October to April

https://doi.org/10.5194/essd-2026-626
Preprint. Discussion started: 8 September 2026

4.4 Temporal variation of snow depths on Arctic sea ice

Temporal variations of SD estimates from the SYSU SnowDepth dataset are examined. As a comparison, results of other five SD products from model-based reconstructions and satellite-based retrievals are also presented. The model-based products comprise simulated SD products from the distributed snow evolution model (SnowModel-LG) (Liston et al., 2020; Stroeve et al., 2020) and NESOSIM (Petty et al., 2018). The satellite-based products consist of the Bremen SnowDepth product derived from AMSR-E/2 (Rostosky et al., 2018), the GSFC SnowDepth product derived from SMMR and SSM/I (Markus and Cavalieri, 1998), the NSIDC SnowDepth product derived from AMSR-E/2 (Comiso et al., 2003).

Figure 7 displays the time series (1978–2025) of monthly mean snow depths during winter (October to April) averaged over six common regions (i.e., Central Arctic Ocean, Beaufort Sea, Chukchi Sea, East Siberian Sea, Laptev Sea, and Kara Sea) and over FYI region. The SYSU SnowDepth dataset exhibits a clear seasonal trend, with SD increasing from October to April. This seasonal variation is consistent with both NESOSIM and SnowModel-LG, indicating that the SYSU SnowDepth dataset can effectively capture the snow accumulation process. The Bremen SnowDepth dataset shows negative snow accumulation from March to April in most years, diverging significantly from NESOSIM and SnowModel-LG. In addition, the SYSU SnowDepth dataset also shows strong correlations with NESOSIM and SnowModel-LG, yielding correlation coefficients of 0.86 and 0.83, respectively. The snow accumulation from October to April varies across the products, with the mean values being 8.83 cm, 10.14 cm, and 13.12 cm for SYSU, NESOSIM, and SnowModel-LG, respectively. Although the SYSU SnowDepth dataset shows relatively lower seasonal snow accumulation than SnowModel-LG and NESOSIM, it provides a valuable alternative SD product directly derived from remote sensing data.

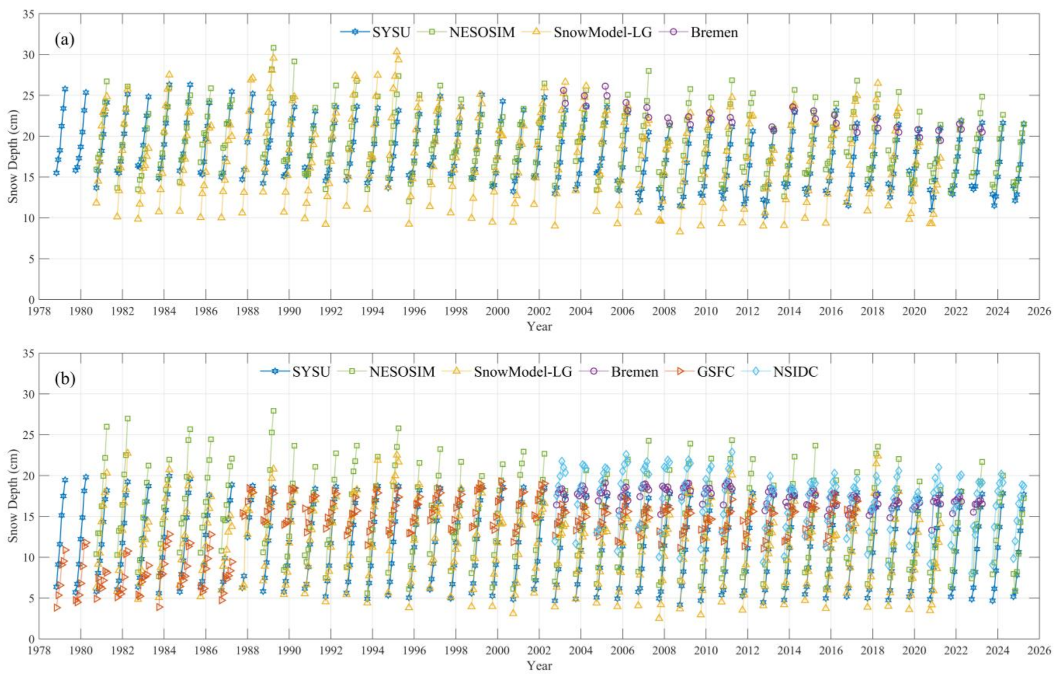

Figure 7. Time series of monthly mean snow depth for different snow depth products from (a) entire region (including Central Arctic Ocean, Beaufort Sea, Chukchi Sea, East Siberian Sea, Laptev Sea and Kara Sea) and (b) first-year ice (FYI) region. Only wintertime (October to April) is shown.

Among the four satellite-based SD products, SYSU is the only one that can provide SD estimates over the entire Arctic (including both FYI and MYI) for the full winter season (October to April). As shown in Figure 7(b), all four SD products could provide SD estimates over FYI. However, notable discrepancies exist among them. Specifically, NSIDC yields the

https://doi.org/10.5194/essd-2026-626
Preprint. Discussion started: 8 September 2026

highest SD with a reasonable accumulation trend, while Bremen shows the lowest snow accumulation during the winter season. Although both the SYSU and GSFC datasets are derived from the SMMR, SSM/I, and SSMIS TB series, SYSU yields more consistent SD estimates than GSFC. Notably, GSFC exhibits a pronounced underestimation of SD during the SMMR period (November 1978 to April 1987), which is likely due to the SMMR TB data not being calibrated to the subsequent SSM/I data.

5 Accuracy evaluation

5.1 Validation with airborne measurements

Three airborne SD datasets, namely, OIB-NSIDC, OIB-GSFC, and AWI-IceBird, are utilized for accuracy evaluation, which relies on three key error metrics: the correlation coefficient (*r*), the mean bias (Bias), and the root-mean-square error (RMSE). While the bias quantifies systematic error, the RMSE reflects the overall magnitude of the differences between the datasets. The minimum airborne transect length required within a given 25 km grid cell was set to 10 km.

Figure 8 presents the density scatterplots comparing the estimated snow depths from the SYSU dataset against the three airborne validation datasets. The SYSU SD estimates strongly correlate with the airborne SD measurements, with correlation coefficient (*r*) values ranging from 0.69 to 0.80. Furthermore, the RMSE values range from 5.93 to 6.79 cm, confirming the high accuracy and robust performance of the SYSU dataset. The mean bias values vary from 0.37 cm to 1.57 cm, indicating a minimal systematic error.

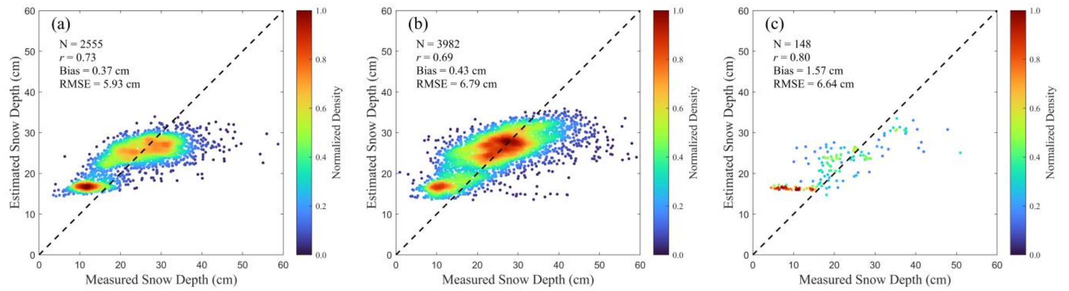

Figure 8. Density scatterplots between estimated and observed snow depth for (a) OIB-NSIDC (2009-2012), (b) OIB-GSFC (2012-2019), and (c) AWI-IceBird (2017 and 2019).

To evaluate the performances of the SYSU dataset across different ice types, Table 4 summarizes the accuracy metrics for both FYI and MYI. Over FYI, SYSU performs well overall, yielding an average RMSE of about 5.87 cm and showing the strongest agreement with OIB-NSIDC (RMSE of 5.46 cm). However, FYI exhibits a notable positive mean bias of about 3.29 cm, indicating that SYSU tends to overestimate SD on this ice type. In contrast, MYI has a relatively poor accuracy with RMSE ranging between 6.04 cm and 7.15 cm alongside a slight negative bias of about −0.25 cm. This larger discrepancy over MYI aligns with the higher uncertainty shown in Table 2 and Table 3. It should be noted that all the airborne SD measurements were obtained in the spring (March to April).

https://doi.org/10.5194/essd-2026-626
Preprint. Discussion started: 8 September 2026

Table 4. Accuracy evaluations using three airborne snow depth datasets, namely, OIB-NSIDC, OIB-GSFC, and AWI-IceBirD through correlation (*r*), mean bias (Bias), and Root-Mean-Square Error (RMSE). *N* indicates the number of match points.

Ice Type	Metrics	OIB-NSIDC	OIB-GSFC	AWI-IceBird
FYI	*N*	528	824	68
	r	0.45	0.42	0.66
	Bias (cm)	3.73	2.60	3.55
	RMSE (cm)	5.46	6.19	5.97
MYI & AMI	*N*	2027	3158	80
	r	0.48	0.53	0.65
	Bias (cm)	-0.51	-0.13	-0.12
	RMSE (cm)	6.04	6.93	7.15

5.2 Validation with buoy measurements

SD measurements from three buoy datasets, including CRREL IMB (2002–2015), AWI SB (2013–2024), and SIMBA (2012–2023), were utilized for validation. To ensure statistical robustness, only buoys with more than 30 coincident data points between the buoy and PMW SD measurements were included, and accuracy metrics were calculated for each buoy individually. A total of 134 buoys were finally selected, consisting of 45 CRREL IMBs (Table A1), 48 AWI SBs (Table A2), and 41 SIMBA buoys (Table A3). The buoy SD measurements span the entire winter season from October to April.

Figure 9 presents density scatterplots comparing the SYSU estimated snow depths against the three buoy datasets, alongside histograms of the accuracy metrics (i.e., *r*, Bias and RMSE) calculated for the 134 individual buoys. Compared to the airborne SD measurements, accuracy degraded slightly with RMSE values ranging between 9.93 cm and 16.75 cm. This finding aligns with previous studies (Zhou et al., 2021; He et al., 2023; Zhou et al., 2025), and likely stems from the lower spatial representativeness of point-based buoy measurements relative to wide-area airborne data. While airborne data can provide high-resolution, small-scale SD measurements along the flight trajectory with high spatial representativeness, buoys are sparsely distributed. Therefore, they only capture local SD at the deployment site and fail to reflect the broader variations (Shalina and Sandven, 2018; Kilic et al., 2019; Koo et al., 2021). This spatial mismatch could introduce a pronounced representativeness error when validating satellite-derived footprints against localized, point-scale buoy data.

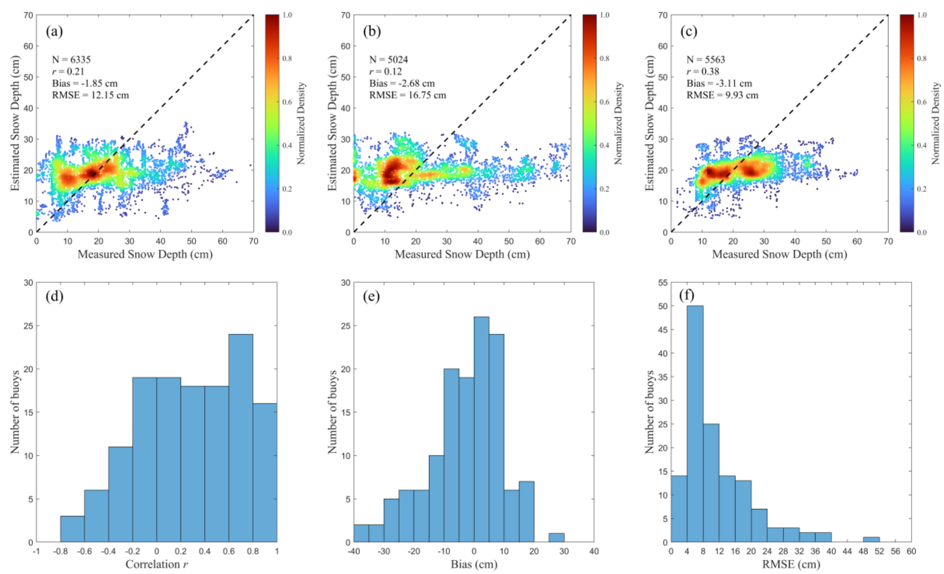

Figure 9. Density scatterplots between estimated and observed snow depth for (a) CRREL IMB (2002–2015), (b) AWI SB (2013–2024), and (c) SIMBA (2012–2023) and histograms of evaluation metrics for (d) correlation (*r*), (e) mean bias (Bias) and (f) RMSE.

https://doi.org/10.5194/essd-2026-626
Preprint. Discussion started: 8 September 2026

Histograms of accuracy metrics demonstrate that the SYSU SD estimates significantly (p < 0.05) correlate with 75 buoys, while 89 buoys fall within a ±10 cm bias range. Furthermore, the RMSE values follow a normal distribution with a median of 8.62 cm, and approximately 80% of the buoys (103 out of 134) exhibit an RMSE below 16.00 cm. The above results indicate that the SYSU SD estimates agree well with the majority of the buoy measurements and offer reasonable accuracy.

SD measurements from the MOSAiC buoy array and transect measurements were also utilized to validate the SYSU SnowDepth dataset. Compared to individual buoys, the buoy array generally offers greater spatial representativeness. Figure 10 displays the temporal evolution of SD from both in situ measurements and SYSU satellite estimates, along with the corresponding scatterplots between the estimated and measured values. During the MOSAiC freezing season, both in situ observations and SYSU satellite estimates show a gradual increase in SD from October 2019 to April 2020, reflecting seasonal snow accumulation over Arctic sea ice. The buoy array record provides a relatively continuous temporal reference and shows substantial sub-grid-scale variability, as indicated by the broad ±1 standard deviation envelope. While the SYSU SD estimates broadly reproduce the seasonal increase in SD, they are generally higher than the buoy array measurements throughout most of the observation period, particularly during the middle and late winter months. In contrast, the SYSU estimates are typically lower than the transect measurements. This difference likely reflects the distinct spatial representativeness of the two in situ datasets: buoy array measurements provide continuous point-based observations, whereas transect measurements sample spatially distributed snow conditions and may better capture thicker snow features associated with local redistribution and deformation. Overall, the SYSU SnowDepth product successfully captures the seasonal evolution of SD during MOSAiC and aligns well with in situ observations, yielding RMSE values of 2.86 cm against the buoy array and 3.99 cm against transect measurements.

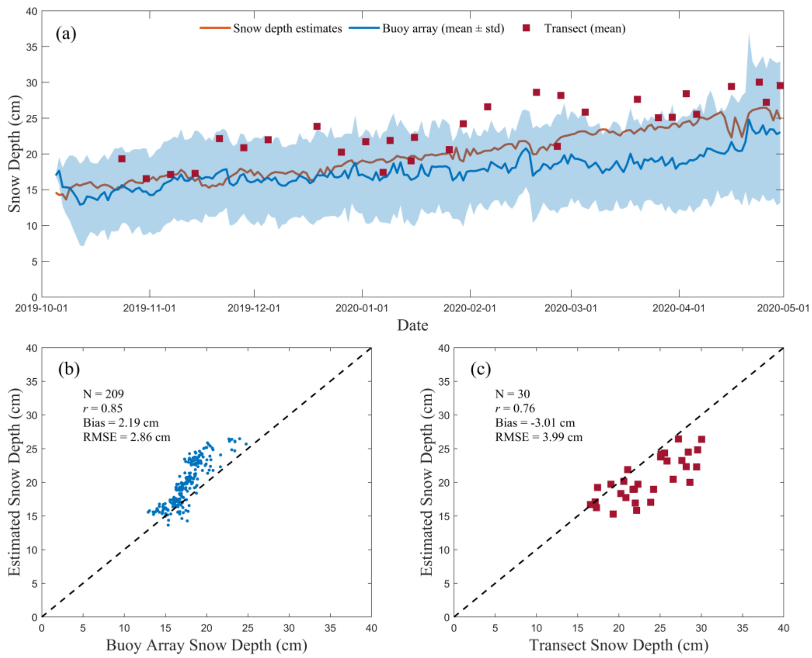

Figure 10. Comparison between buoy array snow depth observations and snow depth estimates during the MOSAiC expedition from October 2019 to April 2020. (a) Temporal evolution of snow depth derived from SYSU satellite estimates, buoy array measurements, and transect observations; (b) Scatterplot comparisons between PMW snow depth and in situ observations for buoy array measurements; (d) scatterplot between snow depth estimates and transect measurements.

https://doi.org/10.5194/essd-2026-626
Preprint. Discussion started: 8 September 2026

5.3 Validation with aircraft landing and ship-based measurements

The aircraft landing SD measurements (Romanov, 2004) and ASSIST/IceWatch ship-based observations (Kern, 2020; Hutchings et al., 2018) were also utilized for SD validation. Figure 11 shows the spatial distribution of the two in situ SD measurements and their corresponding density scatterplots. For the aircraft landing and ASSIST/IceWatch datasets, the validation yields RMSE values of 11.58 cm and 12.26 cm, respectively, which are comparable to the individual buoy validation results shown in Figure 9. For the aircraft landing dataset, a positive bias of 7.94 cm can be observed, occurring primarily over shallow snow covers (SD less than 15 cm). This overestimation is consistent with the trends seen for FYI in Table 4, indicating that the SYSU product tends to overestimate SD over FYI during March and April. For the ASSIST/IceWatch dataset, an overall bias of -0.32 cm is observed. However, a closer look into the validation results across different months reveals that the biases for shallow snow covers are 0.79 cm, 9.22 cm, and 10.64 cm, for October, March, and April, respectively. This indicates the overestimation primarily occurs during late winter months (March and April) whereas the bias remains minimal in early winter (October).

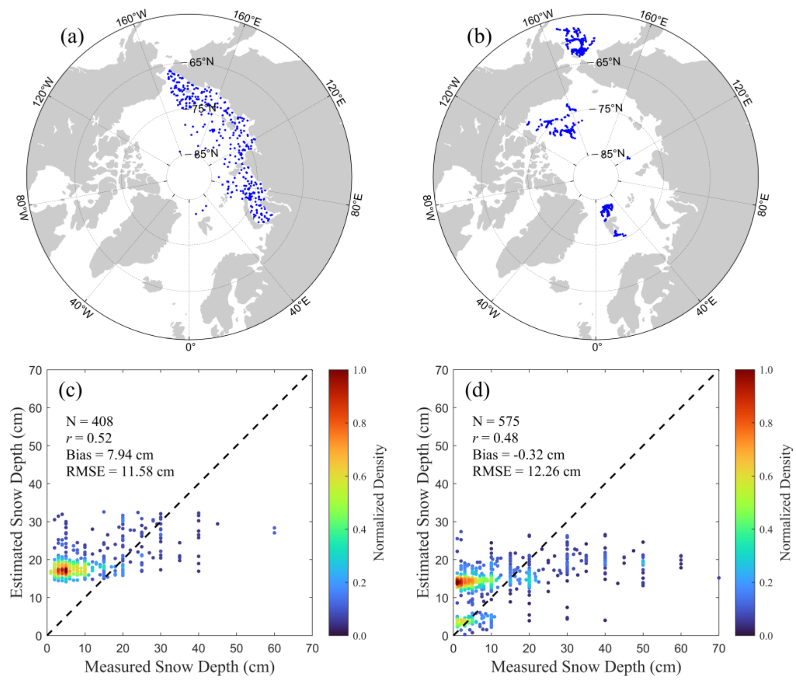

Figure 11. Spatial distribution of in situ measurements for (a) aircraft landing observations (1979–1988) (b) ASSIST/IceWatch data (2003–2018), and density scatterplots between estimated snow depth and in situ measured snow depth for (c) aircraft landing observations and (d) ASSIST/IceWatch data.

6 Discussion

6.1 Influence of spatial representativeness on validation results

In this study, a variety of SD reference observations were utilized to evaluate the SYSU SnowDepth dataset, including airborne, individual buoy, buoy array, aircraft landing, and ship-based datasets. While individual buoy and aircraft landing observations provide point-scale measurements, airborne and ship-based data offer transect-based observations. Since the evaluation performance strongly depends on the type and spatial scale of the reference data as demonstrated by the preceding results, the influences of spatial representativeness on the validation results were further investigated based on transect-based

https://doi.org/10.5194/essd-2026-626
Preprint. Discussion started: 8 September 2026

SD observations (i.e., OIB-NSIDC, OIB-GSFC, and ASSIST/IceWatch). For the airborne datasets, spatial representativeness can be represented by the transect length of the flight trajectory within a 25 km pixel. For ship-based observations, it is quantified by the number of data points located within a single 25 km grid cell. Generally, longer transects and larger counts of data points correspond to higher spatial representativeness.

Figure 12 displays the RMSE values and corresponding validation sample sizes across different levels of spatial representativeness, using data from OIB-NSIDC, OIB-GSFC, and ASSIST/IceWatch. Generally, the RMSE shows a downward trend as spatial representativeness increases. The only exception is an increase in RMSE at a transect length of 25 km for airborne datasets, which may be attributed to the relatively small number of validation data points available at this scale. These findings demonstrate that higher spatial representativeness directly improves validation accuracy, which can also be confirmed by comparing the individual buoy results (Figure 9) with those of the buoy array (Figure 10). Therefore, when evaluated against highly representative reference data, the SYSU SnowDepth dataset is expected to achieve a low RMSE of approximately 6.50 cm.

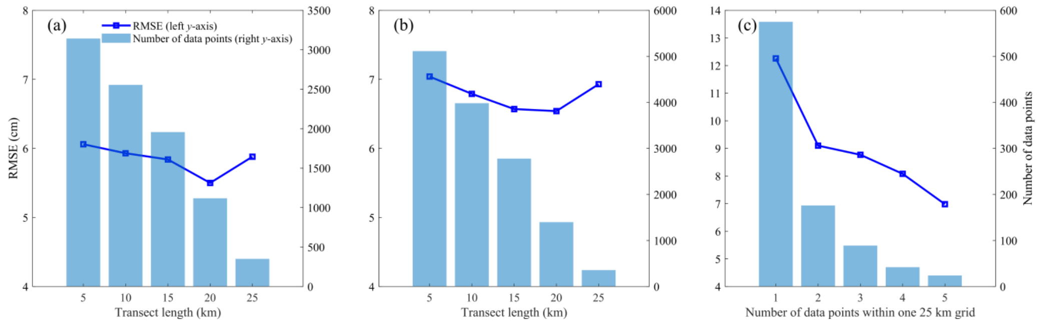

Figure 12. Validation metrics versus different transect lengths for (a) OIB-NSIDC, (b) OIB-GSFC, and verse different number of data point for (c) ASSIST/IceWatch.

6.2 Seasonal variation of retrieval accuracy

Among the various SD reference datasets, most are limited to measurements in specific months. In contrast, individual buoy observations cover the entire winter season (October to April), enabling an evaluation of seasonal variations in retrieval accuracy. In this study, a total of 103 buoys with RMSE values below 16.00 cm (as indicated in Figure 9) were selected for further analysis. This threshold was chosen to mitigate low spatial representativeness while maintaining a sufficiently large and robust sample size.

Figure 13 presents the density scatterplot between estimated and measured snow depths over the 103 selected buoys together with the accuracy metrics (i.e., *r*, Bias, and RMSE) across different months. It can be observed that an overall good performance was achieved with RMSE value being 8.26 cm and mean bias being 0.12 cm. The correlation coefficient *r* exhibits a slight downward trend from October to April with mean value being 0.36. Biases remain within ±1.30 cm from October through February, followed by a notable overestimation in March and April. This upward bias is consistent with the overestimation of shallow snow depths in March and April as indicated in Table 4 and Figure 11. Additionally, RMSE values gradually increase from 6.38 cm in October to 10.89 cm in April, which agrees with the trend in SD uncertainties shown in Figure 5.

https://doi.org/10.5194/essd-2026-626
Preprint. Discussion started: 8 September 2026

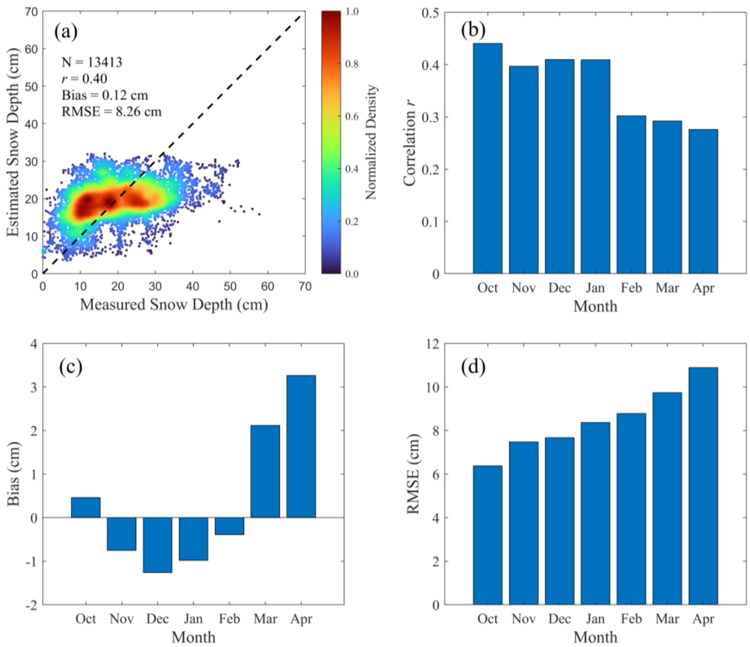

Figure 13. Density scatterplots between estimated and observed snow depth for (a) selected buoys and seasonal variation of accuracy metrics for (b) correlation, (c) Bias, and (d) RMSE.

6.3 Potential uncertainties in snow depth estimates

In this study, GRV(37/19) was utilized to estimate SD on Arctic sea ice. Since GRV(37/19) relies on relatively high frequencies (i.e., 19 and 37 GHz), its signal tends to saturate in deep snow, which may introduce substantial uncertainties in SD estimates. As a result, the maximum retrievable SD is usually limited to 50 cm (Markus et al., 2006). To mitigate these saturation effects, our proposed SD estimation algorithm incorporates two additional variables (i.e., ρ_{snow} and D). To quantify the contributions of these variables to the predicted SD, a permutation feature importance analysis (Breiman, 2001) was performed on the three input parameters, that is, GRV(37/19), ρ_{snow}, and D in Equation (4) and (5). Over FYI, the importance values (measured as the increase in prediction error) were 0.27 cm for GRV(37/19), 0.14 cm for ρ_{snow}, and 1.28 cm for D, identifying D as the dominant predictor. Over MYI, the importance values for the three variables were 0.57 cm, 0.23 cm, and 0.43 cm, respectively, suggesting that all three input features contribute comparably to SD estimation. These results demonstrate that GRV(37/19) is not the sole contributing predictor and the inclusion of ρ_{snow} and D could help mitigate the saturation effects of GRV(37/19) in deep snow. Furthermore, the SYSU SnowDepth dataset could effectively capture both the spatial variations of SD illustrated in Figure 6 and long-term temporal trends which align closely with the two model-based SD products shown in Figure 7. In summary, the impact of GRV(37/19) saturation on deep SD estimation is expected to be minimal for the training dataset with SD below 40 cm.

It should be emphasized that the proposed algorithm is only limited to dry snow conditions. However, winter warm air intrusions (WAIs) over Arctic sea ice have pronounced impacts on SD estimation. WAIs significantly alter radiometer TBs by triggering rapid snow metamorphism and thaw-refreeze cycles (Rostosky and Spreen, 2023; Rückert et al., 2023), and hence directly bias the SD estimates (Comiso et al., 2003; Cavalieri et al., 2012). Furthermore, these WAIs also modify key physical properties of the snowpack and ice (Stroeve et al., 2022; Rückert et al., 2023), such as snow density, grain size, and correlation length, and further compound retrieval uncertainties (He et al., 2024). A 5-day running average method (Comiso et al., 2003; Cavalieri et al., 2012) is commonly employed to mitigate the influence of transient weather and freeze-thaw

https://doi.org/10.5194/essd-2026-626
Preprint. Discussion started: 8 September 2026

events. Additionally, by leveraging a dataset of detected WAIs (Rostosky and Spreen, 2023), SD estimates with potentially high uncertainties can be flagged and treated with caution.

The proposed algorithm relies on distinguishing between FYI and MYI using the C3S sea ice type data, making ice type misclassification a key source of uncertainty. According to Figure 4, the median GRV(37/19) values for FYI and MYI are -0.050 and -0.007, respectively. Misclassifications frequently occur within this overlapping range (-0.050 to -0.007) due to similar microwave emission characteristics. To analyse the potential error induced by ice type misclassification, we calculated the differences in predicted SD using the FYI and MYI models separately. The analysis covered GRV(37/19) values from -0.050 to -0.007 at an interval of 0.001, snow density ρ_{snow} from 0.20 to 0.40 at an interval of 0.01, and D values from 1 to 212 at an interval of 1. The resulting histogram of these differences reveals that the bias (defined as the SD predicted by the MYI model in Equation (9) minus that of the FYI model in Equation (8)) ranges from -1.4 cm to 8.0 cm, with a mean of 2.93 cm. This mean of 2.93 cm represents the overall error level introduced by FYI/MYI misclassifications.

7 Code and data availability

The newly developed SYSU SnowDepth dataset in this study is available at https://doi.org/10.5281/zenodo.21472646 (He et al., 2026). The final data files are formatted as binary files with not-anumber (NaN) denoting missing data. An example to read the data in Matlab is also provided. The Nimbus-7 SMMR polar gridded brightness temperature data were available at https://nsidc.org/data/nsidc-0007/versions/1 (Gloersen, 2006); The DMSP SSM/I-SSMIS daily polar gridded brightness temperature data were available at https://nsidc.org/data/nsidc-0001/versions/4 (Meier et al., 2021); The ICESat-2 and CryoSat-2 L4 Monthly Arctic Snow Depth and Sea Ice Thickness were available at https://nsidc.org/data/nsidc-0773/versions/1 (Kacimi and Kwok, 2022b); The NASA Eulerian Snow On Sea Ice Model Version 1.1 (NESOSIMv1.1) data were available at https://zenodo.org/records/18273881 (Petty, 2026); The Lagrangian Snow Distributions for Sea-Ice Applications, Version 1 were available at https://nsidc.org/data/nsidc-0758/versions/1 (Liston et al., 2021); The NOAA/NSIDC Climate Data Record of Passive Microwave Sea Ice Concentration dataset was available at https://nsidc.org/data/g02202/versions/6 (Meier et al., 2026); The daily gridded sea ice type data were available at https://cds.climate.copernicus.eu/datasets/satellite-sea-ice-edge-type?tab=overview (Aaboe et al., 2023); The NASA GSFC Arctic snow depth on sea ice were available at https://earth.gsfc.nasa.gov/cryo/data/arctic-snow-depth-sea-ice (Markus and Cavalieri, 1998); The AMSR-E/AMSR2 Unified L3 Daily 12.5 km Brightness Temperatures, Sea Ice Concentration, Motion & Snow Depth Polar Grids were available at https://nsidc.org/data/au_si12/versions/1 (Meier et al., 2018); The Winter snow depth on Arctic sea ice from AMSR-E/2 at the University of Bremen were available at https://data.seaice.uni-bremen.de/SnowDepth/ (Rostosky et al., 2018); The Morphometric Characteristics of Ice and Snow in the Arctic Basin: Aircraft Landing Observations from the Former Soviet Union were available at https://nsidc.org/data/g02140/versions/1 (Romanov, 2004); The standardized ASSIST/IceWatch data were available at https://www.cen.uni-hamburg.de/en/icdc/data/cryosphere/seaiceparameter-shipobs.html (Hutchings et al., 2018; Kern, 2020); The IceBridge L4 Sea Ice Freeboard, Snow Depth, and Thickness, Version 1 were available at https://nsidc.org/data/idcsi4/versions/1 (Kurtz et al., 2015); The IceBridge Sea Ice Freeboard, Snow Depth, and Thickness Quick Look, Version 1 were available at https://nsidc.org/data/nsidc-0708/versions/1 (Kurtz et al., 2016); The AWI IceBird snow depth measurements were available at https://doi.org/10.1594/PANGAEA.966009 (Jutila et al., 2024b) and https://doi.org/10.1594/PANGAEA.966057 (Jutila et al., 2024a); The CRREL ice mass balance buoy (IMB) data were available at https://imb-crrel-dartmouth.org/archived-data/ (Perovich et al., 2022); The AWI SB data were available at https://data.seaiceportal.de/relaunch/buoy?lang=en (Nicolaus et al., 2017); The Snow and Ice Mass Balance Array (SIMBA) buoy data were available at https://doi.org/10.1594/PANGAEA.973193 (Preußer et al., 2025).

https://doi.org/10.5194/essd-2026-626
Preprint. Discussion started: 8 September 2026

8 Conclusions

This study proposed a new algorithm for estimating snow depth (SD) on Arctic sea ice based on the spectral gradient ratio (GR) between vertically polarized brightness temperatures (TBs) at 19 and 37 GHz. This algorithm was applied to SMMR, SSM/I, and SSMIS radiometer records to construct a long-term snow depth dataset spanning 1978 to 2025. The newly developed SYSU SnowDepth dataset was then validated against a variety of snow depth reference datasets, including airborne, buoy (individual and array), aircraft landing, and ship-based observations. The impacts of the spatial representativeness, seasonal retrieval accuracy and estimation uncertainties were also assessed. To our knowledge, the SYSU SnowDepth dataset is the longest satellite-based SD product that covers the entire Arctic (encompassing both FYI and MYI regions) for the complete winter season (October to April), and effectively captures both seasonal dynamics and long-term temporal changes.

The relationship between GRV(37/19) derived from SSMIS TB data and altimetric snow depth (ASD) obtained from ICESat-2 and CryoSat-2 freeboard differences was investigated. Results showed that this linear relationship exhibits strong seasonal variation, suggesting that the static linear retrieval models used in earlier NSIDC, GSFC and Bremen SnowDepth products could introduce substantial uncertainty. Therefore, a new snow depth estimation algorithm was proposed by incorporating snow density (ρ_{snow}) from NESOSIM and a time factor (D). This algorithm was trained using a multiple linear regression model on three years of coincident TB and ASD data from 2018–2020. On the training dataset, the algorithm achieved an RMSE of 3.01 cm for FYI and 4.65 cm for MYI. This represents a substantial improvement over a baseline linear regression model excluding the influence of ρ_{snow} and D, which yielded higher RMSE values of 4.41 cm and 5.37 cm for FYI and MYI, respectively. A Gaussian error propagation method was utilized to quantify uncertainties in the snow depth estimates. The resulting uncertainties show a clear upward trend, increasing from 1.97 cm in October to 7.29 cm in April, with MYI consistently exhibiting greater uncertainty than FYI.

To evaluate the newly developed SYSU SnowDepth dataset, a variety of independent reference datasets were utilized, including airborne, buoy (individual buoys and buoy array), aircraft landing, and ship-based observations. These reference data were categorized into point-scale measurements (such as individual buoys, aircraft landing, and ship-based observations) and transect-based measurements (such as airborne and buoy array), with the latter providing a higher level of spatial representativeness. Validation performance was found to be highly sensitive to this spatial representativeness. More specifically, the RMSE values ranged from 2.86 to 6.79 cm for transect-based measurements, but increased to 9.93–16.57 cm for point-scale measurements. While this study leveraged all available snow depth observations for validation, the spatial and temporal sparsity of the reference data prevented a thorough validation with comprehensive coverage of the entire Arctic region and study period. Alternative validation methods like triple collocation analysis (He et al., 2023) require further investigation.

The newly proposed snow depth retrieval algorithm was trained using monthly coincident GRV(37/19) and ASD data due to the limited temporal resolution of ASD data. However, incorporating near-coincident CryoSat-2 and ICESat-2 observations enables estimation of ASD data at daily basis, which would provide a deeper understanding of the relationship between GRV(37/19) and snow depth. Furthermore, the current algorithm was trained on only three years of data, and a longer-term ASD record, which can be derived from combined SARAL/AltiKa and CryoSat-2 data (Carret et al., 2025), will be essential to evaluate its long-term stability and performance.

Appendix A: Overview of all selected buoys in this study

Table A1**.** Overview of all selected ice mass balance buoys (IMBs) in this study (45 in total).

Table A2**.** Overview of all selected snow buoys in this study (41 in total).

Table A3. Overview of all selected Snow and Ice Mass Balance Array (SIMBA) buoys in this study (41 in total).

https://doi.org/10.5194/essd-2026-626
Preprint. Discussion started: 8 September 2026

Open Access Earth System Science Data Discussions

Table A4**.** Overview of all selected MOSAiC buoys in this study (21 in total).

https://doi.org/10.5194/essd-2026-626
Preprint. Discussion started: 8 September 2026

Open Access Earth System Science Data Discussions

Table A1. Overview of all selected ice mass balance buoys (IMBs) in this study (45 in total). Note: The start and end dates correspond to the first and last effective snow depth records.

Buoy name	Start date (YYYY/MM/DD)	End date (YYYY/MM/DD)	Initial snow depth (cm)	Final snow depth (cm)	Mean snow depth (cm)
2002A	2002/04/25	2003/02/28	31	30	18
2003C	2003/08/31	2004/07/10	4	0	18
2003D	2003/08/23	2003/12/01	15	44	31
2004B	2004/04/24	2005/01/11	26	19	17
2004C	2004/04/28	2004/12/08	23	16	12
2004D	2004/04/25	2005/03/07	12	29	17
2004E	2004/08/31	2005/05/26	0	24	23
2005C	2005/08/15	2006/08/19	0	0	6
2005F	2005/09/03	2007/03/18	0	50	11
2006B	2006/04/25	2007/01/20	48	36	38
2006C	2006/09/04	2007/06/13	21	11	41
2006D	2006/09/04	2007/12/02	0	45	21
2006E	2006/09/05	2007/06/17	1	27	14
2007C	2007/05/01	2007/12/13	5	65	22
2009F	2009/09/07	2010/03/01	0	25	20
2009G	2009/10/07	2010/01/27	19	12	12
2010A	2010/04/20	2010/11/20	24	37	23
2010F	2010/10/08	2011/06/16	28	17	28
2010H	2010/10/25	2011/07/26	0	7	4
2011A	2011/03/25	2011/06/02	0	1	1
2011I	2011/08/05	2012/01/20	2	2	8
2011J	2011/08/06	2012/05/18	1	20	9
2011K	2011/08/09	2012/05/16	0	159	16
2011M	2011/09/29	2013/04/22	6	43	19
2012G	2012/10/01	2013/12/23	17	86	34
2012H	2012/09/10	2013/09/26	2	2	15
2012I	2012/08/14	2012/12/21	10	43	30
2012J	2012/08/25	2013/08/03	0	16	24
2012L	2012/08/27	2013/08/28	2	3	8
2012M	2012/08/29	2013/08/14	0	0	31
2013B	2013/04/10	2013/12/17	2	20	8
2013F	2013/08/25	2015/08/13	2	26	33
2013G	2013/9/04	2014/05/05	2	20	18
2013H	2013/09/03	2013/12/29	5	5	7
2013I	2013/09/24	2014/02/12	6	21	15
2014B	2014/03/26	2014/07/29	3	0	5
2014C	2014/03/20	2014/08/24	20	0	24
2014E	2014/04/11	2015/01/03	19	51	24
2014F	2014/08/11	2015/07/06	1	0	10
2014I	2014/10/09	2015/08/22	23	6	17
2015B	2015/03/26	2015/06/08	6	4	6
2015D	2015/04/10	2016/02/01	5	119	25
2015F	2015/08/13	2016/08/02	7	2	16
2015G	2015/09/13	2016/02/22	8	18	19
2015J	2015/09/28	2016/07/07	4	11	21

https://doi.org/10.5194/essd-2026-626
Preprint. Discussion started: 8 September 2026

Open Access Earth System Science Data Discussions

645 **Table A2. Overview of all selected snow buoys in this study (48 in total). Note: The start and end dates correspond to the first and last effective snow depth records.**

Buoy name	Start date (YYYY/MM/DD)	End date (YYYY/MM/DD)	Initial snow depth (cm)	Final snow depth (cm)	Mean snow depth (cm)
2013S4	2013/03/15	2013/06/11	3	0	9
2014S13	2014/03/30	2014/06/23	0	1	3
2014S14	2014/04/01	2014/07/02	34	18	33
2014S15	2014/08/29	2014/12/31	1	53	11
2014S25	2014/09/28	2015/08/23	1	0	25
2015S16	2015/09/19	2016/07/15	8	0	28
2015S20	2015/09/14	2016/04/19	11	20	22
2015S21	2015/09/25	2016/06/19	0	6	3
2015S22	2015/03/01	2015/05/06	37	46	43
2015S29	2015/09/27	2016/07/01	8	0	14
2015S32	2015/09/11	2016/04/28	6	13	9
2015S35	2015/09/10	2016/02/03	0	32	16
2016S36	2016/09/15	2017/08/25	0	46	28
2016S44	2016/10/06	2017/06/05	6	31	11
2016S45	2016/09/22	2017/05/31	16	61	50
2016S50	2016/10/06	2016/12/25	2	16	4
2018S66	2018/09/02	2018/11/16	4	29	24
2018S70	2018/09/07	2019/05/27	8	63	39
2018S71	2018/09/15	2019/06/30	0	0	11
2018S73	2018/09/11	2019/06/29	0	0	13
2018S74	2018/09/14	2019/06/27	0	0	9
2018S75	2018/09/13	2019/07/06	0	0	9
2018S77	2018/09/11	2019/08/21	0	1	9
2018S78	2018/09/16	2019/06/30	0	0	5
2018S82	2018/08/20	2019/08/24	8	32	103
2018S85	2018/09/17	2018/12/13	8	15	19
2019S79	2019/10/07	2019/11/28	12	13	14
2019S92	2019/10/11	2019/11/26	16	17	17
2019S96	2019/10/29	2020/06/07	0	0	1
2020S98	2020/09/17	2021/07/01	0	126	117
2020S99	2020/02/10	2020/08/06	55	171	37
2020S105	2020/09/21	2021/04/12	2	110	59
2020S106	2020/08/26	2021/06/26	1	36	93
2020S108	2020/08/30	2021/07/07	0	115	78
2022S116	2022/07/14	2023/01/27	2	0	80
2022S121	2022/08/27	2023/03/03	3	152	88
2023S100	2023/09/09	2024/02/26	19	167	104
2023S122	2023/08/31	2024/08/28	2	7	15
2023S123	2023/08/25	2024/06/27	0	0	11
2023S124	2023/08/30	2024/05/17	69	29	50
2023S125	2023/08/30	2024/06/16	2	51	43
2023S127	2023/08/28	2024/06/16	0	35	30
2023S128	2023/08/31	2024/03/29	36	164	87
2024S131	2024/09/08	2025/07/05	0	5	25
2024S137	2024/09/25	2025/03/30	4	26	20
2024S138	2024/09/23	2025/03/22	18	43	36
2024S139	2024/09/17	2025/06/01	9	19	16
2024S140	2024/09/19	2025/05/16	20	33	56

https://doi.org/10.5194/essd-2026-626
Preprint. Discussion started: 8 September 2026

Open Access Earth System Science Data Discussions

Table A3. Overview of all selected Snow and Ice Mass Balance Array (SIMBA) buoys in this study (41 in total). Note: The start and end dates correspond to the first and last effective snow depth records.

Buoy name	Start date (YYYY/MM/DD)	End date (YYYY/MM/DD)	Initial snow depth (cm)	Final snow depth (cm)	Mean snow depth (cm)
2012T30	2012/09/09	2012/11/06	2	12	11
2012T31	2012/08/11	2012/11/08	4	26	16
2012T32	2012/08/11	2012/12/21	2	34	19
2014T14	2014/08/26	2015/05/10	10	58	41
2014T33	2014/08/27	2015/04/08	12	36	30
2015T19	2015/09/08	2016/04/28	14	26	23
2015T20	2015/09/25	2016/03/22	7	12	14
2015T22	2015/09/02	2015/11/21	2	30	15
2015T23	2015/09/12	2016/01/28	21	22	29
2015T25	2015/09/12	2016/03/19	12	24	24
2016T39	2016/10/06	2016/11/17	20	24	21
2018T35	2018/09/14	2019/07/11	0	8	20
2018T46	2018/09/16	2019/07/13	0	18	10
2018T51	2018/08/23	2019/03/21	6	30	22
2018T52	2018/09/14	2019/07/19	0	30	11
2018T53	2018/09/12	2019/07/01	0	6	16
2018T54	2018/09/11	2019/07/07	0	16	12
2018T55	2018/09/15	2019/08/31	0	14	11
2019T57	2019/10/07	2019/11/30	14	20	18
2020T60	2020/01/08	2020/03/29	12	8	12
2020T78	2020/08/23	2021/02/25	4	44	27
2020T81	2020/08/30	2020/12/27	1	34	25
2020T84	2020/08/26	2021/03/19	3	37	23
2020T85	2020/09/19	2021/06/11	6	22	12
2022T94	2022/08/12	2023/01/26	11	32	24
2022T95	2022/08/01	2023/02/01	3	26	13
2022T96	2022/07/28	2022/11/21	4	44	20
2022T97	2022/08/06	2022/11/21	7	32	11
2022T98	2022/08/27	2023/02/06	4	26	12
2023T99	2023/08/26	2024/02/25	4	26	26
2023T100	2023/09/13	2024/03/04	9	36	20
2023T102	2023/09/05	2023/11/14	3	20	14
2023T104	2023/08/09	2023/11/21	6	22	10
2023T105	2023/09/01	2024/06/20	3	14	16
2023T106	2023/08/28	2024/06/17	4	32	32
2023T107	2023/09/03	2024/04/10	10	36	32
2023T109	2023/08/29	2024/01/11	6	24	22
2023T110	2023/09/10	2024/01/20	9	60	41
2023T111	2023/08/31	2024/04/09	24	38	29
2023T112	2023/08/17	2024/02/29	6	24	23
2023T114	2023/08/15	2024/02/03	14	48	29

Table A4. Overview of all selected MOSAiC buoys in this study (21 in total), including the Snow and Ice Mass Balance Apparatus (SIMBA), Seasonal Ice Mass Balance buoy (SIMB), and Snow buoy (Snow). Note: The start and end dates correspond to the first and last effective snow depth records.

Buoy name	Start date (YYYY/MM/DD)	End date (YYYY/MM/DD)	Initial snow depth (cm)	Final snow depth (cm)	Mean snow depth (cm)
2019T47	2019/10/13	2020/02/07	10	14	15
2019T56	2019/11/02	2020/04/30	16	18	15
2019T58	2019/10/08	2020/04/30	12	14	15
2019T62	2019/10/30	2020/04/30	20	26	21
2019T63	2019/10/07	2020/04/28	14	22	19
2019T64	2019/10/10	2020/04/30	16	26	20
2019T65	2019/10/08	2020/04/30	14	30	23
2019T66	2019/10/30	2020/04/30	10	8	13
2019T67	2019/11/09	2020/04/30	22	24	23
2019T68	2019/10/05	2020/04/30	17	21	24
2019T69	2019/10/12	2020/01/31	8	26	17
2019T70	2019/10/10	2020/04/30	6	20	14
2019T72	2019/10/09	2020/04/27	14	28	15
SIMB-L1	2019/10/06	2020/03/15	16	24	23
SIMB-L2	2019/10/07	2020/04/30	15	28	23
SIMB-L3	2019/10/10	2020/01/30	6	7	6
2019S81	2019/10/07	2020/04/30	13	13	14
2019S86	2019/10/13	2020/04/30	23	36	28
2019S87	2019/10/14	2020/04/11	11	9	10
2019S93	2019/10/07	2020/04/30	13	14	14
2019S94	2019/10/11	2020/04/30	9	45	15

Author contributions

LH designed the experiments and XP carried them out. LH and XP prepared the manuscript with contributions from all co-authors. YZ, FH, ZC, LC, WX, and XC contributed to the discussion and provided valuable comments.

Competing interests

The contact author has declared that none of the authors has any competing interests.

Disclaimer

Publisher’s note: Copernicus Publications remains neutral with regard to jurisdictional claims made in the text, published maps, institutional affiliations, or any other geographical representation in this paper. While Copernicus Publications makes every effort to include appropriate place names, the final responsibility lies with the authors.

Acknowledgements

The authors would like to thank all the data providers for their data. The authors also acknowledge the use of AI-based language tools (Gemini) to improve the clarity, grammar, and overall readability of this manuscript. These tools were used strictly for language refinement without altering the scientific content and conclusions.

Financial support

This study was supported by the National Key Research and Development Program of China (Grant No. 2024YFB3908005) and Guangdong Basic and Applied Basic Research Foundation (Grant No. 2024A1515012007).

References

Aaboe, S., Down, E. J., Sørensen, A., Lavergne, T., and Eastwood, S.: Sea-ice type climate data record 1978-present, v3.0, Copernicus Climate Change Service (C3S) Climate Data Store (CDS) [dataset], https://doi.org/10.24381/cds.29c46d83, 2023.

Arduini, G., Keeley, S., Day, J. J., Sandu, I., Zampieri, L., and Balsamo, G.: On the Importance of Representing Snow Over Sea-Ice for Simulating the Arctic Boundary Layer, Journal of Advances in Modeling Earth Systems, 14, e2021MS002777, https://doi.org/10.1029/2021MS002777, 2022.

Braakmann-Folgmann, A. and Donlon, C.: Estimating snow depth on Arctic sea ice using satellite microwave radiometry and a neural network, The Cryosphere, 13, 2421-2438, https://doi.org/10.5194/tc-13-2421-2019, 2019.

Breiman, L.: Random Forests, Machine Learning, 45, 5-32, https://doi.org/10.1023/A:1010933404324, 2001.

Carret, A., Fleury, S., Di Bella, A., Landy, J., Lawrence, I., Kurtz, N., Laforge, A., Bouffard, J., and Parrinello, T.: A multi-frequency altimetry snow depth product over Arctic sea ice, Scientific Data, 12, 104, 10.1038/s41597-024-04343-4, 2025.

Cavalieri, D. J., Gloersen, P., and Campbell, W. J.: Determination of sea ice parameters with the NIMBUS 7 SMMR, Journal of Geophysical Research: Atmospheres, 89, 5355-5369, https://doi.org/10.1029/JD089iD04p05355, 1984.

Cavalieri, D. J., Markus, T., Ivanoff, A., Miller, J. A., Brucker, L., Sturm, M., Maslanik, J. A., Heinrichs, J. F., Gasiewski, A. J., Leuschen, C., Krabill, W., and Sonntag, J.: A Comparison of Snow Depth on Sea Ice Retrievals Using Airborne Altimeters and an AMSR-E Simulator, IEEE Trans. Geosci. Remote Sens., 50, 3027-3040, https://doi.org/10.1109/TGRS.2011.2180535, 2012.

Comiso, J. C.: Characteristics of Arctic winter sea ice from satellite multispectral microwave observations, Journal of Geophysical Research: Oceans, 91, 975-994, https://doi.org/10.1029/JC091iC01p00975, 1986.

Comiso, J. C., Cavalieri, D. J., and Markus, T.: Sea ice concentration, ice temperature, and snow depth using AMSR-E data, IEEE Trans. Geosci. Remote Sens., 41, 243-252, https://doi.org/10.1109/TGRS.2002.808317, 2003.

Dai, L., Che, T., and Ding, Y.: Inter-Calibrating SMMR, SSM/I and SSMI/S Data to Improve the Consistency of Snow-Depth Products in China, https://doi.org/10.3390/rs70607212, 2015.

Fritzner, S., Graversen, R., Christensen, K. H., Rostosky, P., and Wang, K.: Impact of assimilating sea ice concentration, sea ice thickness and snow depth in a coupled ocean–sea ice modelling system, The Cryosphere, 13, 491-509, https://doi.org/10.5194/tc-13-491-2019, 2019.

Gloersen, P.: Nimbus-7 SMMR Polar Gridded Radiances and Sea Ice Concentrations, Version 1, NASA National Snow and Ice Data Center Distributed Active Archive Center [dataset], https://doi.org/10.5067/QOZIVYV3V9JP, 2006.

He, L., Xue, B., Hui, F., and Cheng, X.: Triple Collocation-Based Merging of Winter Snow Depth Retrievals on Arctic Sea Ice Derived From Three Different Algorithms Using AMSR2, IEEE Trans. Geosci. Remote Sens., 61, 1-15, https://doi.org/10.1109/TGRS.2023.3290073, 2023.

He, L., Xue, B., Huang, S., Hui, F., Chen, Z., and Cheng, X.: On the Synergy of SMAP and AMSR2 for Estimating Snow Depth on Arctic Sea Ice, IEEE Geosci. Remote Sens. Lett., 19, 1-5, https://doi.org/10.1109/LGRS.2022.3188001, 2022.

https://doi.org/10.5194/essd-2026-626
Preprint. Discussion started: 8 September 2026

He, L., Xue, B., Hui, F., Xu, S., Chen, Z., and Cheng, X.: Toward Daily Snow Depth Estimation on Arctic Sea Ice During the Whole Winter Season From Passive Microwave Radiometer Data, IEEE Trans. Geosci. Remote Sens., 62, 1-15, https://doi.org/10.1109/TGRS.2024.3358340, 2024.

He, L., Peng, X., Zhou, Y., Hui, F., Chen, Z., Chen, L., Wang, X., and Cheng, X.: A long-term wintertime snow depth dataset on Arctic sea ice (1978-2025) derived from multisource passive microwave radiometer data, Zenodo [dataset], https://doi.org/10.5281/zenodo.21472646, 2026.

Huber, P. J.: Robust Statistics, Wiley, https://doi.org/10.1002/0471725250, 1981.

Hutchings, J., Delamere, J., and Heil, P.: The Ice Watch Manual, 2018.

Intergovernmental Panel on Climate, C.: Climate Change 2021 – The Physical Science Basis: Working Group I Contribution to the Sixth Assessment Report of the Intergovernmental Panel on Climate Change, Cambridge University Press, Cambridge, https://doi.org/10.1017/9781009157896, 2023.

Itkin, P., Hendricks, S., Webster, M., von Albedyll, L., Arndt, S., Divine, D., Jaggi, M., Oggier, M., Raphael, I., Ricker, R., Rohde, J., Schneebeli, M., and Liston, G. E.: Sea ice and snow characteristics from year-long transects at the MOSAiC Central Observatory, Elementa: Science of the Anthropocene, 11, 00048, https://doi.org/10.1525/elementa.2022.00048, 2023.

Ivanova, N., Pedersen, L. T., Tonboe, R. T., Kern, S., Heygster, G., Lavergne, T., Sørensen, A., Saldo, R., Dybkjær, G., Brucker, L., and Shokr, M.: Inter-comparison and evaluation of sea ice algorithms: towards further identification of challenges and optimal approach using passive microwave observations, The Cryosphere, 9, 1797-1817, https://doi.org/10.5194/tc-9-1797-2015, 2015.

Jutila, A., Hendricks, S., Ricker, R., von Albedyll, L., and Haas, C.: Airborne sea ice parameters during the IceBird Winter 2019 campaign in the Arctic Ocean, Version 2, https://doi.org/10.1594/PANGAEA.966057, 2024a.

Jutila, A., Hendricks, S., Ricker, R., von Albedyll, L., and Haas, C.: Airborne sea ice parameters during the PAMARCMIP2017 campaign in the Arctic Ocean, Version 2, https://doi.org/10.1594/PANGAEA.966009, 2024b.

Kacimi, S. and Kwok, R.: Arctic Snow Depth, Ice Thickness, and Volume From ICESat-2 and CryoSat-2: 2018–2021, Geophysical Research Letters, 49, e2021GL097448, https://doi.org/10.1029/2021GL097448, 2022a.

Kacimi, S. and Kwok, R.: ICESat-2 and CryoSat-2 L4 Monthly Arctic Snow Depth and Sea Ice Thickness, Version 1, NASA National Snow and Ice Data Center Distributed Active Archive Center [dataset], https://doi.org/10.5067/04YYIKXW0GJS, 2022b.

Kern, S.: ESA-CCI Phase2 Standardized Manual Visual Ship-Based Sea Ice Observations v02, World Data Center for Climate (WDCC) at DKRZ [dataset], https://doi.org/10.26050/WDCC/ESACCIPSMVSBSIOV2, 2020.

Kern, S., Khvorostovsky, K., Skourup, H., Rinne, E., Parsakhoo, Z. S., Djepa, V., Wadhams, P., and Sandven, S.: The impact of snow depth, snow density and ice density on sea ice thickness retrieval from satellite radar altimetry: results from the ESA-CCI Sea Ice ECV Project Round Robin Exercise, The Cryosphere, 9, 37-52, https://doi.org/10.5194/tc-9-37-2015, 2015.

Kilic, L., Tonboe, R. T., Prigent, C., and Heygster, G.: Estimating the snow depth, the snow–ice interface temperature, and the effective temperature of Arctic sea ice using Advanced Microwave Scanning Radiometer 2 and ice mass balance buoy data, The Cryosphere, 13, 1283-1296, https://doi.org/10.5194/tc-13-1283-2019, 2019.

Koo, Y., Lei, R., Cheng, Y., Cheng, B., Xie, H., Hoppmann, M., Kurtz, N. T., Ackley, S. F., and Mestas-Nuñez, A. M.: Estimation of thermodynamic and dynamic contributions to sea ice growth in the Central Arctic using ICESat-2 and MOSAiC SIMBA buoy data, Remote Sens. Environ., 267, 112730, https://doi.org/10.1016/j.rse.2021.112730, 2021.

Kurtz, N., Studinger, M., Harbeck, J., Onana, V.-D.-P., and Yi, D.: IceBridge L4 Sea Ice Freeboard, Snow Depth, and Thickness, Version 1, NASA National Snow and Ice Data Center Distributed Active Archive Center [dataset], https://doi.org/10.5067/G519SHCKWQV6, 2015.

https://doi.org/10.5194/essd-2026-626
Preprint. Discussion started: 8 September 2026

Open Access Earth System Science Data Discussions

Kurtz, N., Studinger, M., Harbeck, J., Onana, V.-D.-P., and Yi, D.: IceBridge Sea Ice Freeboard, Snow Depth, and Thickness Quick Look, Version 1, NASA National Snow and Ice Data Center Distributed Active Archive Center [dataset], https://doi.org/10.5067/GRIXZ91DE0L9, 2016.

Kwok, R. and Markus, T.: Potential basin-scale estimates of Arctic snow depth with sea ice freeboards from CryoSat-2 and ICESat-2: An exploratory analysis, Advances in Space Research, 62, 1243-1250, https://doi.org/10.1016/j.asr.2017.09.007, 2018.

Kwok, R., Kacimi, S., Webster, M. A., Kurtz, N. T., and Petty, A. A.: Arctic Snow Depth and Sea Ice Thickness From ICESat-2 and CryoSat-2 Freeboards: A First Examination, Journal of Geophysical Research: Oceans, 125, e2019JC016008, https://doi.org/10.1029/2019JC016008, 2020.

Kwon, Y. J., Kim, H. C., Kim, J. M., Park, J. W., and Kim, S. H.: Sensitivity of Passive Microwave Satellite Observations to Snow Density and Grain Size Over Arctic Sea Ice, IEEE Trans. Geosci. Remote Sens., 61, 1-10, https://doi.org/10.1109/TGRS.2023.3322401, 2023.

Landy, J. C., de Rijke-Thomas, C., Nab, C., Lawrence, I., Glissenaar, I. A., Mallett, R. D. C., Fredensborg Hansen, R. M., Petty, A., Tsamados, M., Macfarlane, A. R., and Braakmann-Folgmann, A.: Anticipating CRISTAL: an exploration of multi-frequency satellite altimeter snow depth estimates over Arctic sea ice, 2018–2023, The Cryosphere, 20, 183-208, https://doi.org/10.5194/tc-20-183-2026, 2026.

Lee, S.-M., Shi, H., Sohn, B.-J., Gasiewski, A. J., Meier, W. N., and Dybkjær, G.: Winter Snow Depth on Arctic Sea Ice From Satellite Radiometer Measurements (2003–2020): Regional Patterns and Trends, Geophysical Research Letters, 48, e2021GL094541, https://doi.org/10.1029/2021GL094541, 2021.

Lei, R., Cheng, B., Hoppmann, M., and Zuo, G.: Snow depth and sea ice thickness derived from the measurements of SIMBA buoys deployed in the Arctic Ocean during the Legs 1a, 1, and 3 of the MOSAiC campaign in 2019-2020, https://doi.org/10.1594/PANGAEA.938244, 2021.

Li, H., Ke, C., Zhu, Q., Li, M., and Shen, X.: A deep learning approach to retrieve cold-season snow depth over Arctic sea ice from AMSR2 measurements, Remote Sens. Environ., 269, 112840, https://doi.org/10.1016/j.rse.2021.112840, 2022.

Liston, G., Stroeve, J., and Itkin, P.: Lagrangian Snow Distributions for Sea-Ice Applications, Version 1, NASA National Snow and Ice Data Center Distributed Active Archive Center [dataset], https://doi.org/10.5067/27A0P5M6LZBI, 2021.

Liston, G. E., Itkin, P., Stroeve, J., Tschudi, M., Stewart, J. S., Pedersen, S. H., Reinking, A. K., and Elder, K.: A Lagrangian Snow-Evolution System for Sea-Ice Applications (SnowModel-LG): Part I—Model Description, Journal of Geophysical Research: Oceans, 125, e2019JC015913, https://doi.org/10.1029/2019JC015913, 2020.

Liu, J., Zhang, Y., Cheng, X., and Hu, Y.: Retrieval of Snow Depth over Arctic Sea Ice Using a Deep Neural Network, Remote Sensing, 11, 2864, https://doi.org/10.3390/rs11232864, 2019.

Maaß, N., Kaleschke, L., Tian-Kunze, X., and Drusch, M.: Snow thickness retrieval over thick Arctic sea ice using SMOS satellite data, The Cryosphere, 7, 1971-1989, https://doi.org/10.5194/tc-7-1971-2013, 2013.

Mallett, R. D. C., Stroeve, J. C., Tsamados, M., Landy, J. C., Willatt, R., Nandan, V., and Liston, G. E.: Faster decline and higher variability in the sea ice thickness of the marginal Arctic seas when accounting for dynamic snow cover, The Cryosphere, 15, 2429-2450, https://doi.org/10.5194/tc-15-2429-2021, 2021.

Markus, T. and Cavalieri, D. J.: Snow Depth Distribution Over Sea Ice in the Southern Ocean from Satellite Passive Microwave Data, in: Antarctic Sea Ice: Physical Processes, Interactions and Variability, 19-39, https://doi.org/10.1029/AR074p0019, 1998.

Markus, T., Powell, D. C., and Wang, J. R.: Sensitivity of passive microwave snow depth retrievals to weather effects and snow evolution, IEEE Trans. Geosci. Remote Sens., 44, 68-77, https://doi.org/10.1109/TGRS.2005.860208, 2006.

https://doi.org/10.5194/essd-2026-626
Preprint. Discussion started: 8 September 2026

Meier, W., Markus, T., and Comiso, J.: AMSR-E/AMSR2 Unified L3 Daily 12.5 km Brightness Temperatures, Sea Ice Concentration, Motion & Snow Depth Polar Grids, Version 1, NASA National Snow and Ice Data Center Distributed Active Archive Center [dataset], https://doi.org/10.5067/RA1MIJOYPK3P, 2018.

Meier, W., Fetterer, F., Windnagel, A., Stewart, J. S., and Stafford, T.: NOAA/NSIDC Climate Data Record of Passive Microwave Sea Ice Concentration, Version 6, National Snow and Ice Data Center [dataset], https://doi.org/10.7265/B18J-Z797, 2026.

Meier, W., Stewart, J., Wilcox, H., Scott, D., and Hardman, M.: DMSP SSM/I-SSMIS Daily Polar Gridded Brightness Temperatures, Version 6, NASA National Snow and Ice Data Center Distributed Active Archive Center [dataset], https://doi.org/10.5067/MXJL42WSXTS1, 2021.

Nelson, C., Stroeve, J., Lavergne, T., Landy, J., Willatt, R., Johnson, T., Baordo, F., Mallett, R., and Tsamados, M.: Snow Depth on Arctic Sea Ice Retrieval Using a Synergy of Sentinel-3's Active and Passive Microwave Instruments, Geophysical Research Letters, 53, e2025GL121068, https://doi.org/10.1029/2025GL121068, 2026.

Nicolaus, M., Hoppmann, M., Arndt, S., Hendricks, S., Katlein, C., König-Langlo, G., Nicolaus, A., Rossmann, L., Schiller, M., Schwegmann, S., Langevin, D., and Bartsch, A.: Snow height and air temperature on sea ice from Snow Buoy measurements, https://doi.org/10.1594/PANGAEA.875638, 2017.

Nicolaus, M., Perovich, D. K., Spreen, G., Granskog, M. A., von Albedyll, L., Angelopoulos, M., Anhaus, P., Arndt, S., Belter, H. J., Bessonov, V., Birnbaum, G., Brauchle, J., Calmer, R., Cardellach, E., Cheng, B., Clemens-Sewall, D., Dadic, R., Damm, E., de Boer, G., Demir, O., Dethloff, K., Divine, D. V., Fong, A. A., Fons, S., Frey, M. M., Fuchs, N., Gabarró, C., Gerland, S., Goessling, H. F., Gradinger, R., Haapala, J., Haas, C., Hamilton, J., Hannula, H.-R., Hendricks, S., Herber, A., Heuzé, C., Hoppmann, M., Høyland, K. V., Huntemann, M., Hutchings, J. K., Hwang, B., Itkin, P., Jacobi, H.-W., Jaggi, M., Jutila, A., Kaleschke, L., Katlein, C., Kolabutin, N., Krampe, D., Kristensen, S. S., Krumpen, T., Kurtz, N., Lampert, A., Lange, B. A., Lei, R., Light, B., Linhardt, F., Liston, G. E., Loose, B., Macfarlane, A. R., Mahmud, M., Matero, I. O., Maus, S., Morgenstern, A., Naderpour, R., Nandan, V., Niubom, A., Oggier, M., Oppelt, N., Pätzold, F., Perron, C., Petrovsky, T., Pirazzini, R., Polashenski, C., Rabe, B., Raphael, I. A., Regnery, J., Rex, M., Ricker, R., Riemann-Campe, K., Rinke, A., Rohde, J., Salganik, E., Scharien, R. K., Schiller, M., Schneebeli, M., Semmling, M., Shimanchuk, E., Shupe, M. D., Smith, M. M., Smolyanitsky, V., Sokolov, V., Stanton, T., Stroeve, J., Thielke, L., Timofeeva, A., Tonboe, R. T., Tavri, A., Tsamados, M., Wagner, D. N., Watkins, D., Webster, M., and Wendisch, M.: Overview of the MOSAiC expedition: Snow and sea ice, Elementa: Science of the Anthropocene, 10, https://doi.org/10.1525/elementa.2021.000046, 2022.

Perovich, D., Richter-Menge, J., and Polashenski, C.: Observing and understanding climate change: Monitoring the mass balance, motion, and thickness of Arctic sea ice [dataset], 2022.

Perovich, D., Raphael, I., Moore, R., Clemens-Sewall, D., Lei, R., Sledd, A., and Polashenski, C.: Sea ice heat and mass balance measurements from four autonomous buoys during the MOSAiC drift campaign, Elementa: Science of the Anthropocene, 11, https://doi.org/10.1525/elementa.2023.00017, 2023.

Perovich, D. K., Grenfell, T. C., Light, B., and Hobbs, P. V.: Seasonal evolution of the albedo of multiyear Arctic sea ice, Journal of Geophysical Research: Oceans, 107, SHE 20-21-SHE 20-13, https://doi.org/10.1029/2000JC000438, 2002.

Petty, A.: NASA Eulerian Snow On Sea Ice Model Version 1.1 (NESOSIMv1.1) data: 1980 - 2025, Zenodo [dataset], https://doi.org/10.5281/zenodo.18273881, 2026.

Petty, A. A., Webster, M., Boisvert, L., and Markus, T.: The NASA Eulerian Snow on Sea Ice Model (NESOSIM) v1.0: initial model development and analysis, Geosci. Model Dev., 11, 4577-4602, https://doi.org/10.5194/gmd-11-4577-2018, 2018.

Preußer, A., Nicolaus, M., and Hoppmann, M.: Snow depth, sea ice thickness and interface temperatures derived from measurements of SIMBA buoys deployed in the Arctic Ocean and Southern Ocean between 2012 and 2023, https://doi.org/10.1594/PANGAEA.973193, 2025.

https://doi.org/10.5194/essd-2026-626
Preprint. Discussion started: 8 September 2026

Rabe, B., Cox, C. J., Fang, Y.-C., Goessling, H., Granskog, M. A., Hoppmann, M., Hutchings, J. K., Krumpen, T., Kuznetsov, I., Lei, R., Li, T., Maslowski, W., Nicolaus, M., Perovich, D., Persson, O., Regnery, J., Rigor, I., Shupe, M. D., Sokolov, V., Spreen, G., Stanton, T., Watkins, D. M., Blockley, E., Buenger, H. J., Cole, S., Fong, A., Haapala, J., Heuzé, C., Hoppe, C. J. M., Janout, M., Jutila, A., Katlein, C., Krishfield, R., Lin, L., Ludwig, V., Morgenstern, A., O'Brien, J., Zurita, A. Q., Rackow, T., Riemann-Campe, K., Rohde, J., Shaw, W., Smolyanitsky, V., Solomon, A., Sperling, A., Tao, R., Toole, J., Tsamados, M., Zhu, J., and Zuo, G.: The MOSAiC Distributed Network: Observing the coupled Arctic system with multidisciplinary, coordinated platforms, Elementa: Science of the Anthropocene, 12, https://doi.org/10.1525/elementa.2023.00103, 2024.

Romanov, I. P.: Morphometric Characteristics of Ice and Snow in the Arctic Basin: Aircraft Landing Observations from the Former Soviet Union, 1928-1989, https://doi.org/10.7265/N5B8562T, 2004.

Rostosky, P. and Spreen, G.: Relevance of warm air intrusions for Arctic satellite sea ice concentration time series, The Cryosphere, 17, 3867-3881, https://doi.org/10.5194/tc-17-3867-2023, 2023.

Rostosky, P., Spreen, G., Farrell, S. L., Frost, T., Heygster, G., and Melsheimer, C.: Snow Depth Retrieval on Arctic Sea Ice From Passive Microwave Radiometers—Improvements and Extensions to Multiyear Ice Using Lower Frequencies, Journal of Geophysical Research: Oceans, 123, 7120-7138, https://doi.org/10.1029/2018JC014028, 2018.

Rückert, J. E., Rostosky, P., Huntemann, M., Clemens-Sewall, D., Ebell, K., Kaleschke, L., Lemmetyinen, J., Macfarlane, A. R., Naderpour, R., Stroeve, J., Walbröl, A., and Spreen, G.: Sea ice concentration satellite retrievals influenced by surface changes due to warm air intrusions: A case study from the MOSAiC expedition, Elementa: Science of the Anthropocene, 11, 00039, https://doi.org/10.1525/elementa.2023.00039, 2023.

Shalina, E. V. and Sandven, S.: Snow depth on Arctic sea ice from historical in situ data, The Cryosphere, 12, 1867-1886, https://doi.org/10.5194/tc-12-1867-2018, 2018.

Shen, X., Ke, C. Q., and Li, H.: Snow depth product over Antarctic sea ice from 2002 to 2020 using multisource passive microwave radiometers, Earth Syst. Sci. Data, 14, 619-636, https://doi.org/10.5194/essd-14-619-2022, 2022.

Shi, H., Sohn, B.-J., Dybkjær, G., Tonboe, R. T., and Lee, S.-M.: Simultaneous estimation of wintertime sea ice thickness and snow depth from space-borne freeboard measurements, The Cryosphere, 14, 3761-3783, 10.5194/tc-14-3761-2020, 2020.

Sievers, I., Skourup, H., and Rasmussen, T. A. S.: Impact assessment of snow thickness, sea ice density and water density in CryoSat-2-derived sea ice thickness, The Cryosphere, 18, 5985-6004, https://doi.org/10.5194/tc-18-5985-2024, 2024.

Stroeve, J., Liston, G. E., Buzzard, S., Zhou, L., Mallett, R., Barrett, A., Tschudi, M., Tsamados, M., Itkin, P., and Stewart, J. S.: A Lagrangian Snow Evolution System for Sea Ice Applications (SnowModel-LG): Part II—Analyses, Journal of Geophysical Research: Oceans, 125, e2019JC015900, https://doi.org/10.1029/2019JC015900, 2020.

Stroeve, J., Nandan, V., Willatt, R., Dadic, R., Rostosky, P., Gallagher, M., Mallett, R., Barrett, A., Hendricks, S., Tonboe, R., McCrystall, M., Serreze, M., Thielke, L., Spreen, G., Newman, T., Yackel, J., Ricker, R., Tsamados, M., Macfarlane, A., Hannula, H. R., and Schneebeli, M.: Rain on snow (ROS) understudied in sea ice remote sensing: a multi-sensor analysis of ROS during MOSAiC (Multidisciplinary drifting Observatory for the Study of Arctic Climate), The Cryosphere, 16, 4223-4250, https://doi.org/10.5194/tc-16-4223-2022, 2022.

Sturm, M., Perovich, D. K., and Holmgren, J.: Thermal conductivity and heat transfer through the snow on the ice of the Beaufort Sea, Journal of Geophysical Research: Oceans, 107, SHE 19-11-SHE 19-17, https://doi.org/10.1029/2000JC000409, 2002.

Warren, S. G., Rigor, I. G., Untersteiner, N., Radionov, V. F., Bryazgin, N. N., Aleksandrov, Y. I., and Colony, R.: Snow Depth on Arctic Sea Ice, Journal of Climate, 12, 1814-1829, https://doi.org/10.1175/1520-0442(1999)012%3C1814:SDOASI%3E2.0.CO;2, 1999.

Webster, M. A., Parker, C., Boisvert, L., and Kwok, R.: The role of cyclone activity in snow accumulation on Arctic sea ice, Nature Communications, 10, 5285, https://doi.org/10.1038/s41467-019-13299-8, 2019.

https://doi.org/10.5194/essd-2026-626
Preprint. Discussion started: 8 September 2026

Zhou, L., Stroeve, J., Xu, S., Petty, A., Tilling, R., Winstrup, M., Rostosky, P., Lawrence, I. R., Liston, G. E., Ridout, A., Tsamados, M., and Nandan, V.: Inter-comparison of snow depth over Arctic sea ice from reanalysis reconstructions and satellite retrieval, The Cryosphere, 15, 345-367, https://doi.org/10.5194/tc-15-345-2021, 2021.

Zhou, Y., Wang, X., Lei, R., Zhang, C., and Zhang, Y.: AdaSA-SD (v1.0): An Adaptive Seasonal Algorithm for Snow Depth Retrieval Over Arctic Sea Ice, IEEE Trans. Geosci. Remote Sens., 63, 1-22, https://doi.org/10.1109/TGRS.2025.3593433, 2025.

Zhou, Y., Zhang, C., Petty, A., Wang, X., Lei, R., Liu, W., and Zhang, Y.: Enhanced Retrieval of Spring Snow Depth Over Pan-Arctic Sea Ice From AMSR2 Observations for 2013–2023 Using Multi-Model Machine Learning, Journal of Geophysical Research: Machine Learning and Computation, 3, e2026JH001239, https://doi.org/10.1029/2026JH001239, 2026.

Zygmuntowska, M., Rampal, P., Ivanova, N., and Smedsrud, L. H.: Uncertainties in Arctic sea ice thickness and volume: new estimates and implications for trends, The Cryosphere, 8, 705-720, https://doi.org/10.5194/tc-8-705-2014, 2014.